Released bacterial ATP shapes local and systemic inflammation during abdominal sepsis

Daniel Spari[1,2], Annina Schmid[1,2], Daniel Sanchez-Taltavull[1,2], Shaira Murugan[1,2], Keely Keller[1,2], Nadia Ennaciri[1,2], Lilian Salm[1,2], Deborah Stroka[1,2], Guido Beldi[1,2]*

[1]Department of Visceral Surgery and Medicine, Inselspital, Bern University Hospital, University Hospital of Bern, Bern, Switzerland; [2]Department for BioMedical Research, Visceral Surgery and Medicine, University Hospital of Bern, Bern, Switzerland

*For correspondence:
guido.beldi@insel.ch

Abstract Sepsis causes millions of deaths per year worldwide and is a current global health priority declared by the WHO. Sepsis-related deaths are a result of dysregulated inflammatory immune responses indicating the need to develop strategies to target inflammation. An important mediator of inflammation is extracellular adenosine triphosphate (ATP) that is released by inflamed host cells and tissues, and also by bacteria in a strain-specific and growth-dependent manner. Here, we investigated the mechanisms by which bacteria release ATP. Using genetic mutant strains of *Escherichia coli* (*E. coli*), we demonstrate that ATP release is dependent on ATP synthase within the inner bacterial membrane. In addition, impaired integrity of the outer bacterial membrane notably contributes to ATP release and is associated with bacterial death. In a mouse model of abdominal sepsis, local effects of bacterial ATP were analyzed using a transformed *E. coli* bearing an arabinose-inducible periplasmic apyrase hydrolyzing ATP to be released. Abrogating bacterial ATP release shows that bacterial ATP suppresses local immune responses, resulting in reduced neutrophil counts and impaired survival. In addition, bacterial ATP has systemic effects via its transport in outer membrane vesicles (OMV). ATP-loaded OMV are quickly distributed throughout the body and upregulated expression of genes activating degranulation in neutrophils, potentially contributing to the exacerbation of sepsis severity. This study reveals mechanisms of bacterial ATP release and its local and systemic roles in sepsis pathogenesis.

eLife assessment

This **fundamental** study advances our understanding of the role of bacterial-derived extracellular ATP in the pathogenesis of sepsis. The evidence supporting the conclusions is **compelling**, although not all concerns from a previous round of reviews were adequately addressed. The work will be of broad interest to researchers on microbiology and infectious diseases.

Introduction

Worldwide, 11 million sepsis-related deaths were reported in 2017, which accounted for an estimated 19.7% of all global deaths (*Rudd et al., 2020*). Given its high incidence and immense socio-economic burden, the World Health Organization (WHO) has declared sepsis as a global health priority (*Reinhart et al., 2017*).

Sepsis is defined as life-threatening organ dysfunction caused by an imbalanced host immune response to infection. Antibiotic treatment remains the main approach to treat sepsis; however, despite the use of broad-spectrum antibiotics, lethality remains high. Immune-modulating strategies are an additional

eLife digest Sepsis is a severe condition often caused by the body's immune system overreacting to bacterial infections. This can lead to excessive inflammation which damages organs and requires urgent medical care. With sepsis claiming millions of lives each year, new and improved ways to treat this condition are urgently needed. One potential strategy for treating sepsis is to target the underlying mechanisms controlling inflammation.

Inflamed and dying cells release molecules called ATP (the energy carrier of all living cells), which strongly influence the immune system, including during sepsis. In the early stages of an infection, ATP acts as a danger signal warning the body that something is wrong. However, over time, it can worsen infections by disturbing the immune response.

Similar to human cells, bacteria release their own ATP, which can have different impacts depending on the type of bacteria and where they are located in the body. However, it is not well understood how bacterial ATP influences severe infections like sepsis.

To investigate this question, Spari et al analysed how ATP is released from *Escherichia coli*, a type of bacteria that causes severe infections. This revealed that the bacteria secrete ATP directly in to their environment and via small membrane-bound structures called vesicles.

Spari et al. then probed a mouse model of abdominal sepsis which had been infected with *E. coli* that release either normal or low levels of ATP. They found that the ATP released from *E. coli* impaired the mice's survival and lowered the number of neutrophils (immune cells which are important for defending against bacteria) at the site of the infection. The ATP secreted via vesicles also altered the role of neutrophils but in more distant regions, and it is possible that these changes may be contributing to the severity of sepsis.

These findings provide a better understanding of how ATP released from bacteria impacts the immune system during sepsis. While further investigation is needed, these findings may offer new therapeutic targets for treating sepsis.

approach to antibiotics to curb excessive inflammation and to support an effective defense against the infectious agents. Until recently however, most trials inhibiting cytokine responses or Toll-like receptors failed, indicating that alternative approaches for immunomodulation are required (*Cao et al., 2023*).

It has been shown that adenosine triphosphate (ATP), as soon as it is released into the extracellular space, critically modulates inflammatory and immune responses (*Di Virgilio et al., 2020*; *Eltzschig et al., 2012*) by activating ionotropic P2X and metabotropic P2Y receptors (*Burnstock, 2020*; *Junger, 2011*). Also, such purinergic signaling critically alters immune responses during sepsis (*Dosch et al., 2019*; *Ledderose et al., 2016*; *Spari and Beldi, 2020*). In particular, we have described that the connexin-dependent release of ATP by macrophages initiates an autocrine loop of over-activation, resulting in altered local and systemic cytokine secretion, which exacerbates abdominal sepsis (*Dosch et al., 2019*). Such sepsis-promoting effects of host-derived extracellular ATP are secondary to inflammation initiated by bacterial pathogens.

Recently, it has been discovered that also bacteria release ATP into the extracellular space (*Mempin et al., 2013*). Such ATP release might be a conserved mechanism of protection from host defense and precede host responses. ATP release has been shown for a variety of bacteria including the sepsis-associated *Escherichia coli* (*E. coli*) and *Klebsiella pneumoniae* (*K. pneumoniae*) from the Proteobacteria phylum or *Enterococcus faecalis* (*E. faecalis*) and *Staphylococcus aureus* (*S. aureus*) from the Firmicutes phylum (*Diekema et al., 2019*; *Hironaka et al., 2013*; *Iwase et al., 2010*; *Mempin et al., 2013*; *Mureșan et al., 2018*).

The mechanisms by which inflammatory and immune responses in the host are modulated by such released bacterial ATP have just begun to be elucidated (*Spari and Beldi, 2020*). In colonized compartments such as the intestine, it has been shown that ATP released by mutualistic bacteria modulates local cellular and secretory immune responses (*Atarashi et al., 2008*; *Perruzza et al., 2017*; *Proietti et al., 2019*) and in the mouth, bacterial ATP release leads to biofilm dispersal and periodontitis (*Ding et al., 2016a*; *Ding and Tan, 2016b*). However, the role of ATP released by bacteria invading non-colonized compartments, such as the abdominal cavity or the blood in the context of local and systemic infections, remains to be determined.
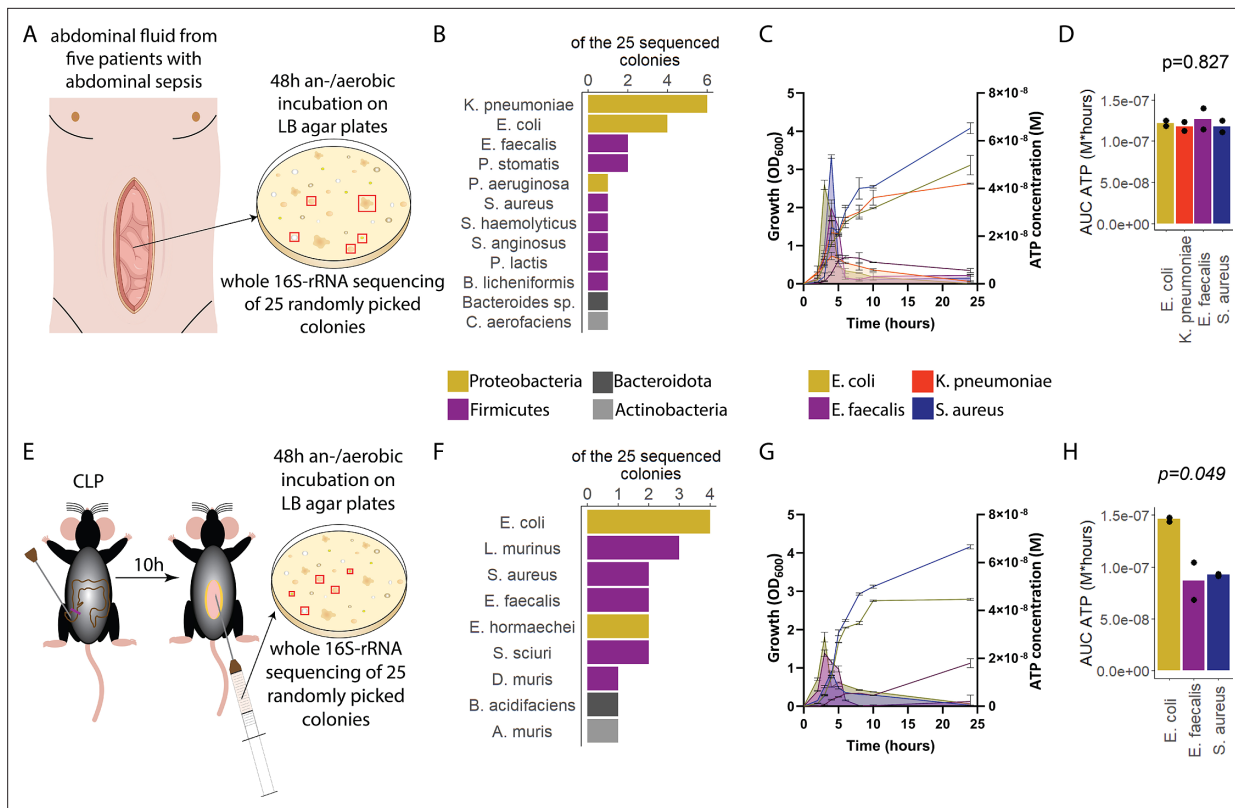
Figure 1. Sepsis-associated bacteria release adenosine triphosphate (ATP) in a growth-dependent manner. (**A**) Experimental approach to isolate and cultivate sepsis-associated bacteria from abdominal fluid of patients with abdominal sepsis. (**B**) Bacterial species identified by whole 16S-rRNA Sanger sequencing from abdominal fluid of patients with abdominal sepsis. Three colonies out of 25 could not be identified. (**C**) Measurement of released ATP (M) and growth (OD_{600}) over time (hours) from the four sepsis-associated bacteria *E. coli*, *K. pneumoniae*, *E. faecalis,* and *S. aureus* isolated from patients. N=2 independent bacteria cultures. Means and standard deviations are shown. (**D**) Area under the curve (AUC) of released ATP over time (M*hours) of the previously assessed bacteria (cumulative ATP). One-way ANOVA, N=2 independent bacteria cultures. Means and individual values are shown. (**E**) Experimental approach to isolate and cultivate sepsis-associated bacteria from abdominal fluid of mice with abdominal sepsis. (**F**) Bacterial species identified by whole 16S-rRNA Sanger sequencing from abdominal fluid of mice with abdominal sepsis. Seven colonies out of 25 could not be identified. (**G**) Measurement of released ATP (M) and growth (OD_{600}) over time (hours) from the three sepsis-associated bacteria *E. coli*, *E. faecalis,* and *S. aureus* isolated from mice. N=2 independent bacteria cultures. Means and standard deviations are shown. (**H**) AUC of released ATP over time (M*hours) of the previously assessed bacteria (cumulative ATP). One-way ANOVA, N=2 independent bacteria cultures. Means and individual values are shown.

The online version of this article includes the following figure supplement(s) for figure 1:

Figure supplement 1. Experimental approach to measure released bacterial adenosine triphosphate (ATP) and growth over time.

In this study, we investigated if ATP released from bacteria influences the outcome of abdominal sepsis. We first isolated sepsis-associated bacteria and measured the amount of ATP they release. Second, we analyzed the function of the inner bacterial membrane on ATP release over time in *E. coli* and in *E. coli* with mutations in integral respiratory chain proteins (*Mempin et al., 2013*). Third, the function of the outer bacterial membrane on ATP release during growth was assessed using porin mutants (*Alvarez et al., 2017*; *Choi and Lee, 2019*). Fourth, we investigated local effects of ATP in the abdominal cavity. Lastly, based on the finding that bacteria secrete outer membrane vesicles (OMV) (*Schwechheimer and Kuehn, 2015*), we investigated systemic consequences of released bacterial ATP.

Results

E. coli, one of the major pathogens in sepsis, releases ATP in a growth-dependent manner

To assess ATP release of sepsis-associated bacteria, abdominal fluid of patients with abdominal sepsis was sampled and an/aerobically incubated on LB agar plates (*Figure 1A*). Twenty-five different colonies were randomly picked and analyzed by whole 16S-rRNA Sanger sequencing, which resulted in 12 different bacterial species (*Figure 1B*). From these, the four most clinically important sepsis-associated bacteria *E. coli*, *K. pneumoniae* (both gram[neg]), *E. faecalis,* and *S. aureus* (both gram[pos]) (*Diekema et al., 2019*; *Mureșan et al., 2018*) were further cultivated for experimental studies. We quantified released ATP over time (*Figure 1—figure supplement 1*) using a luciferin-luciferase-based assay. A growth-dependent release of ATP was observed in all species, peaking during exponential growth phase (*Figure 1C*). Cumulative amount of released ATP was quantified using the area under the curve (AUC) of released ATP over time (AUC ATP). ATP release was detected across all assessed species (*Figure 1D*). To model these findings in mice, abdominal sepsis was induced using a standardized cecal ligation and puncture (CLP) model (*Dosch et al., 2019*; *Figure 1E*). Similar to human samples, Proteobacteria and Firmicutes phyla were predominating (*Figure 1F*, see *Figure 1B*). In the mouse model, *E. coli* released notably more cumulative ATP compared to *E. faecalis* and *S. aureus* (*Figure 1G and H*). The bacterial species assessed in humans and mice (*E. coli*, *E. faecalis*, *S. aureus*) differed on the strain level (sequences deposited, see Data availability statement) confirming that ATP release is strain-specific (*Mempin et al., 2013*). In summary, sepsis-associated bacteria release ATP in a growth-dependent and strain-specific manner. *E. coli,* which is one of the most frequent facultative pathogens in patients with abdominal sepsis, released the highest amount of ATP isolated from a standardized mouse model of abdominal sepsis.

Bacterial ATP release is dependent on ATP synthesis at the inner bacterial membrane and correlates with bacterial growth

After having demonstrated that sepsis-associated bacteria release ATP, we next questioned whether and how ATP release is dependent on ATP generation. ATP synthase and cytochrome oxidases, which are located in the inner bacterial membrane, are key components of ATP generation under aerobic conditions. Therefore, ATP release of the *E. coli* parental strain (PS) was compared to all available mutants of ATP synthase subunits (ΔatpA, ΔatpB, ΔatpC, ΔatpD, ΔatpE, ΔatpF, ΔatpH) and cytochrome bo_3 oxidase subunits (ΔcyoA, ΔcyoB, ΔcyoC, ΔcyoD) from the Keio collection (*Baba et al., 2006*; *Yamamoto et al., 2009*). The use of different mutants allows to identify the most relevant subunits influencing ATP release. Also, it allows to identify a possible correlation of bacterial ATP release with growth, which is a function of ATP generation (*Figure 2A*; *Galber et al., 2021*; *Ihssen et al., 2021*; *Ivancic et al., 2008*; *Lundin, 2000*).

Bacterial growth (OD_{600}) and ATP release were measured over time and cumulative ATP release (AUC ATP) was assessed (*Figure 2B*). We first noticed that mutations in subunits of ATP synthase, which is the key enzyme of ATP generation, were generally associated with significantly lower cumulative ATP release compared to mutations in cytochrome bo_3 oxidase subunits (*Figure 2C*). Therefore, we suspected an interrelation between ATP generation and released ATP (see growth and ATP release curves in *Figure 2B*). We determined cumulative growth (AUC growth) in addition to cumulative ATP release and indeed, cumulative ATP release and cumulative growth were positively correlated (*Figure 2D*), similar to peak ATP and peak growth (OD_{600}) that are positively correlated (*Figure 2—figure supplement 1*). In summary, ATP release is directly dependent on ATP generation at the inner bacterial membrane. Mutations in subunits of bacterial ATP synthase have a higher impact on ATP generation, growth, and ATP release than mutations in subunits of cytochrome bo_3 oxidase (*Figure 2C*).

Outer bacterial membrane integrity and bacterial death determine bacterial ATP release during growth

We next focused on the outer membrane by challenging its integrity while leaving ATP generation and the inner membrane intact. For that purpose, we used the *E. coli* porin mutants ΔompC, ΔompF, ΔlamB, and ΔphoE (*Figure 3A*; *Baba et al., 2006*; *Yamamoto et al., 2009*), which have been shown
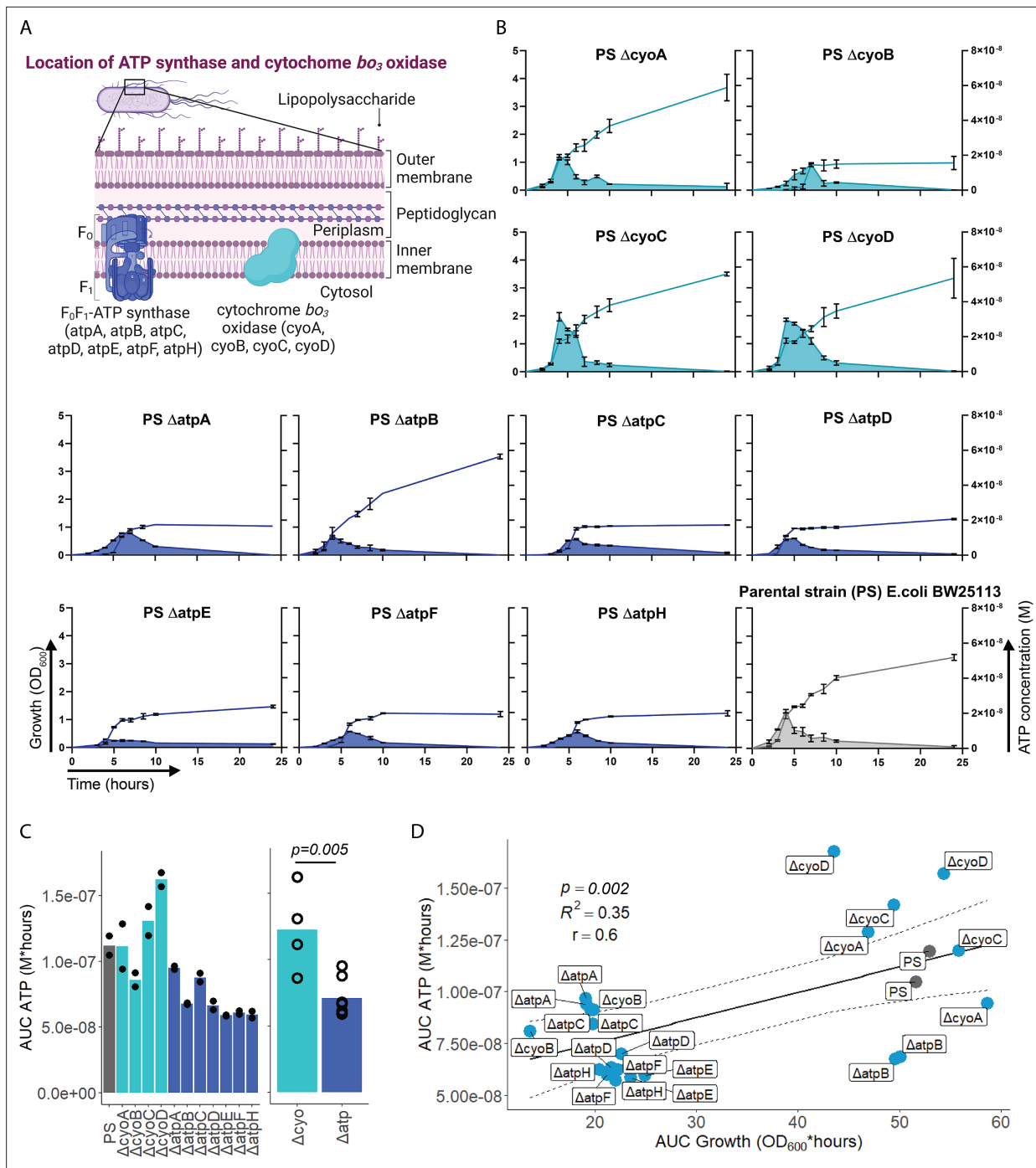
Figure 2. Adenosine triphosphate (ATP) release is dependent on ATP synthesis. (**A**) Illustration depicting the location of ATP synthase and cytochrome *bo₃* oxidase in gram[neg] bacteria. (**B**) Measurement of released ATP (M) and growth (OD_{600}) over time (hours) from cytochrome *bo₃* oxidase (cyo) and ATP synthase (atp) mutants. The parental strain (PS) was added as a control. N=2 independent bacteria cultures. Means and standard deviations are shown. (**C**) Area under the curve (AUC) of released ATP over time (M*hours) of the previously assessed bacteria (cumulative ATP) is shown individually in the left panel. N=2 independent bacteria cultures. Means and individual values are shown. Means of grouped cyo and atp mutants are compared in the right panel. t-Test. Means and individual values are shown. (**D**) Cumulative ATP (M*hours) and cumulative growth (OD_{600}*hours) of all assessed cyo and atp mutants and the PS were plotted against each other. Pearson's correlation (r) and coefficient of determination (R^2) of the applied linear model are depicted. 95% confidence level is shown by the black dashed lines.

© 2024, BioRender Inc. Figure 2A was created using BioRender, and is published under a CC BY-NC-ND 4.0. Further reproductions must adhere to the terms of this license

The online version of this article includes the following figure supplement(s) for figure 2:

Figure 2 continued on next page

to suffer from impaired outer membrane integrity in varying degrees (*Choi and Lee, 2019*). ATP release and growth were measured over time including *E. coli* PS as baseline and membrane destabilizing EDTA and stabilizing Ca^{2+} as additional controls (*Leive, 1968*). Cumulative ATP release (AUC ATP) from the porin mutants were notably different compared to the PS, being lowest in *ΔompC* and highest in *ΔompF* (*Figure 3B and C*).

Interestingly, the *ΔompF* mutant had also a very high peak of released ATP (*Figure 3B*). We hypothesized that this is because of impaired membrane integrity, resulting in ATP release during growth and potentially bacterial death. Thus, we focused on the individual ATP peaks during growth, which were observed after 4 hr of culturing. There was a strong negative correlation between the individual peak of released ATP (marked by the red line in *Figure 3B*) and growth at the same time point (*Figure 3D*).

We did not interfere with ATP generation at the inner membrane but deliberately challenged the outer membrane and tested therewith if destabilization of the outer membrane integrity is associated with bacterial death. Indeed, outer membrane integrity and bacterial death are significantly increased in *ΔompF* compared to *ΔompC* and the PS after 4 hr (ATP peak) of culturing (*Figure 3E and F*), akin to the amount of released ATP (*Figure 3G*). We conclude from these data that destabilization of the outer bacterial membrane (as observed with the *ΔompF* mutant) results in bacterial death that is associated with ATP release.

In summary, outer membrane integrity and finally bacterial death notably contribute to the amount of bacterial ATP release during growth.

Released bacterial ATP reduces neutrophil counts and impairs survival during abdominal sepsis

Next, we wanted to investigate the function of bacterial ATP release in vivo. To study this, we transformed the *E. coli* PS with an arabinose-inducible apyrase (PS+pAPY) and compared it to the PS transformed with the empty vector (PS+pEMPTY) (*Proietti et al., 2019*). In this model, ATP released by bacteria is hydrolyzed and consequently depleted by a periplasmic apyrase (*Santapaola et al., 2006*; *Scribano et al., 2014*).

Indeed, apyrase induction resulted in a significant reduction of ATP release in PS+pAPY, compared to PS+pEMPTY (*Figure 4—figure supplement 1A and B*). To test the consequences in vivo, apyrase was induced by arabinose 3 hr before intraabdominal (i.a.) injection into wild type C57Bl/6 mice (*Figure 4A*). Thereby ATP release was abrogated in the bacteria cultures that were used for injection (*Figure 4B*). In vivo, no difference in ATP levels was detected when ATP was measured directly in the abdominal fluid after 4 (*Figure 4C*) and 8 hr (*Figure 4—figure supplement 1C*). This is not surprising given that ATP is rapidly hydrolyzed by ectonucleotidases in vivo (*Eltzschig et al., 2012*). After both 4 (*Figure 4D and E*) and 8 hr (*Figure 4—figure supplement 1D and E*), no differences in local or systemic bacterial counts were observed. Yet, despite similar bacterial counts, the survival was significantly higher in the absence of bacterial ATP (PS+pAPY) compared to ATP-generating controls (PS+pEMPTY) after i.a. injection (*Figure 4F*).

Next, we asked how this difference in bacterial ATP release affects the immune system. Therefore, inflammatory cells in the abdominal cavity were characterized using flow cytometry (*Figure 4G*). As expected, a disappearance reaction of large peritoneal macrophages (LPM) was observed after both, *E. coli* PS+pEMPTY and *E. coli* PS+pAPY, i.a. injection compared to sham controls after 4 (*Figure 4H*) and 8 hr (*Figure 4—figure supplement 1F*; *Ghosn et al., 2010*). Such LPM disappearance following abdominal *E. coli* infection is a result of free-floating clots composed of LPM and neutrophils and important for effective pathogen clearance (*Salm et al., 2023*; *Vega-Pérez et al., 2021*; *Zindel et al., 2021*) but not dependent on ATP release according to our data. Interestingly, however, the number of small peritoneal macrophages (SPM) and CX3CR1[pos] monocytes was significantly reduced, whereas neutrophils were significantly increased almost up to 8 hr (*Figure 4I*, *Figure 4—figure supplement 1G*) in bacterial ATP-depleted abdominal sepsis (PS+pAPY). This effect is dependent on released bacterial ATP given that no differences in bacterial counts were observed (see *Figure 4D and E*, *Figure 4—figure supplement 1D–E*).
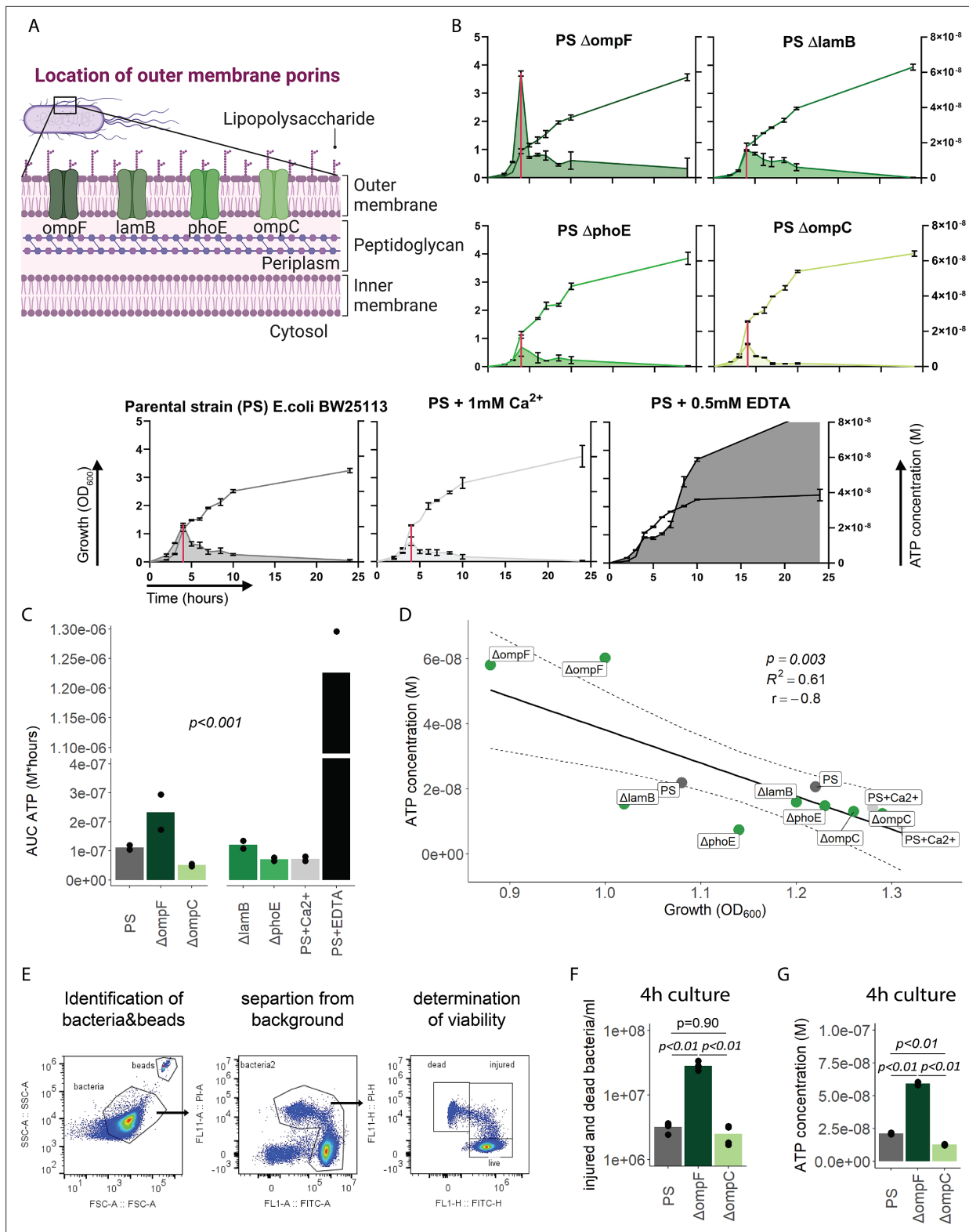
Figure 3. Outer membrane integrity and bacterial death determine bacterial adenosine triphosphate (ATP) release during growth. (**A**) Illustration depicting the location of outer membrane porins in gram[neg] bacteria. (**B**) Measurement of released ATP (M) and growth (OD_{600}) over time (hours) from outer membrane porin mutants. The parental strain (PS) and the PS supplemented with either 1 mM Ca^{2+} or 0.5 mM EDTA were added as controls. N=2 independent bacteria cultures. Means and standard deviations are shown. The red line marks the individual peak of ATP release and growth (OD_{600}) at that time point. (**C**) Area under the curve (AUC) of released ATP over time (M*hours) of the previously assessed bacteria (cumulative ATP). One-way

Figure 3 continued on next page

Figure 3 continued

ANOVA, N=2 independent bacteria cultures. Means and individual values are shown. (**D**) ATP concentration (M) and growth (OD_{600}) at the individual peak of ATP release of all assessed outer membrane porin mutants, the PS, and the PS+Ca^{2+} (no peak for the EDTA control) were plotted against each other. Pearson's correlation (**r**) and coefficient of determination (R^2) of the applied linear model are depicted. 95% confidence level is shown by the black dashed lines. (**E**) Gating strategy to identify added counting beads, live, injured, and dead bacteria. (**F**) Quantitative assessment of injured and dead bacteria, as identified by flow cytometry after 4 hr of culturing (ATP peak) of the PS, $\Delta ompF$ and $\Delta ompC$. One-way ANOVA followed by Tukey post hoc test, N=4 independent bacteria cultures. Means and individual values are shown. (**G**) ATP concentration (M) after 4 hr of culturing (ATP peak) of the PS, $\Delta ompF$ and $\Delta ompC$. One-way ANOVA followed by Tukey post hoc test, N=2 independent bacteria cultures. Means and individual values are shown.

In summary, ATP released by bacteria suppresses abdominal inflammatory responses and worsened survival in a model of abdominal sepsis.

Establishing ATP-loaded OMV as a model system to assess the systemic relevance of bacterial ATP

ATP is rapidly metabolized in the extracellular space and therefore, the mode of action of released bacterial ATP is limited to the immediate cellular vicinity (*Junger, 2011*). However, the outcome of sepsis is not only dependent on local but also on systemic responses to microorganisms. Therefore, we hypothesized that bacterial ATP has systemic effects as protected cargo in OMV (*Alvarez et al., 2017*). OMV are small (20–300 nm) spherical particles that are released by both gram[neg] and gram[pos] bacteria (*Schwechheimer and Kuehn, 2015*). In gram[neg] bacteria, they bulge off the outer membrane and disseminate throughout the body (*Jang et al., 2015*). They are equipped with typical bacterial surface features lacking the machinery for self-reproduction, and contain DNA, proteins, and metabolites (*Baeza and Mercade, 2021*; *Bitto et al., 2017*; *Kulp and Kuehn, 2010*; *Lee et al., 2007*). Therefore, OMV are suited as a systemic delivery system for bacterial ATP. Indeed, recently, ATP has been detected in OMV derived from pathogenic *Neisseria gonorrhoeae*, *Pseudomonas aeruginosa* PAO1, and *Acinetobacter baumannii* AB41 (*Pérez-Cruz et al., 2015*).

To assess the potential of OMV as ATP carriers, we compared the OMV production from several hypervesiculation *E. coli* mutants ($\Delta mlaE$, $\Delta mlaA$, $\Delta rfaD$, $\Delta degP$, $\Delta rodZ$, $\Delta nlpI$, $\Delta tolB$) (*Figure 5A*; *McBroom et al., 2006*). The $\Delta nlpI$ and $\Delta tolB$ strains showed a 20- and 30-fold increase of OMV when compared with the PS (*Figure 5B*). We then assessed ATP release and growth over time from $\Delta nlpI$, $\Delta tolB$, and the PS, to identify their individual peak of ATP release, and isolated OMV at their individual peak of ATP release and after 24 hr (*Figure 5—figure supplement 1A*). ATP was detected in OMV from all assessed strains at the individual peak of ATP release but only in minimal detectable levels after 24 hr (*Figure 5C*). The $\Delta tolB$ OMV isolated after 24 hr were then used as ATP-depleted vehicles. Density gradient ultracentrifugation showed that most $\Delta tolB$ OMV were of similar density and protein composition (*Figure 5D*, *Figure 5—figure supplement 1B*). They were equipped with outer membrane ompF but not cytoplasmic ftsZ (*Figure 5D*), indicating that they are outer membrane derived. In order to generate OMV with known and constant ATP concentrations, we used electroporation (EP) to load OMV with ATP while empty OMV ($\Delta tolB$ OMV harvested from 24 hr culture) served as ATP-depleted controls (*Fu et al., 2020*; *Lennaárd et al., 2021*). Before and after EP, the OMV size distribution was assessed by nanoparticle tracking analysis and morphology by electron microscopy (*Figure 5E*, *Figure 5—figure supplement 1C*). OMV were loaded with ATP (*Figure 5F*) and over time, the amount of ATP in OMV decreased, especially at physiological (37°C) temperature (*Figure 5G*) as opposed to 4°C (*Figure 5—figure supplement 1D*).

In summary, OMV contain ATP and release ATP at physiological temperatures. To use OMV as an ATP delivery system, empty OMV were loaded using EP.

OMV-derived bacterial ATP induces degranulation processes in neutrophils after lysosomal uptake

OMV are potent inducers of inflammation and sepsis (*Park et al., 2010*; *Park et al., 2013*), which travel throughout the body and are taken up by a variety of cells (*Bittel et al., 2021*; *Kim et al., 2013*; *Lee et al., 2018*). To tests the hypothesis that ATP within OMV mediates systemic effects of invasive
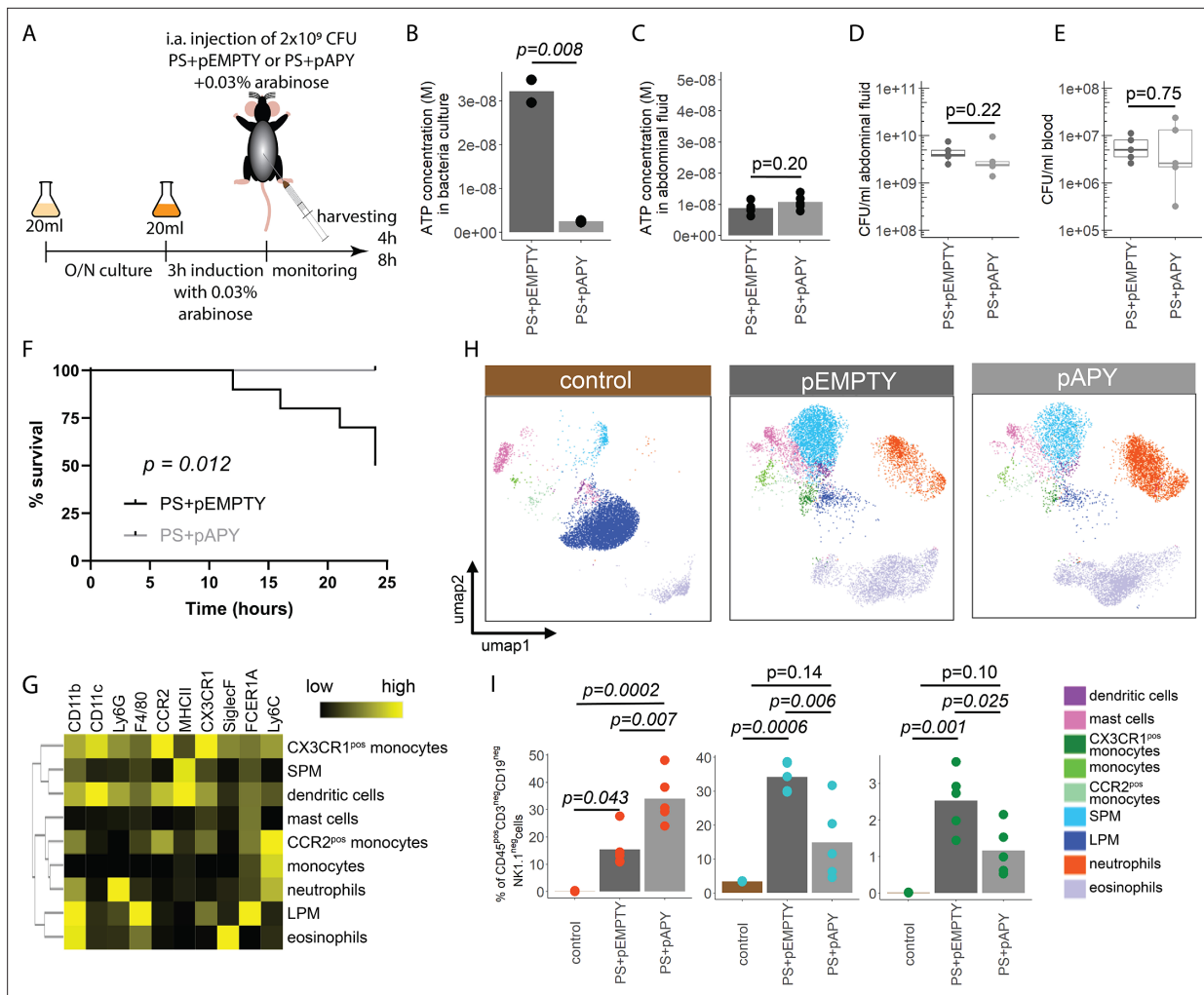
Figure 4. Bacterial adenosine triphosphate (ATP) reduces neutrophil counts and impairs sepsis outcome in vivo. (**A**) Experimental approach to determine the local role of bacterial ATP in vivo, intraabdominal (i.a.) injecting parental strain (PS)+pEMPTY or PS+pAPY. (**B**) Measurement of released ATP (M) in bacteria culture supernatant immediately before bacteria were i.a. injected. t-Test, N=2 independent bacteria cultures. Means and individual values are shown. (**C**) Measurement of ATP (M) in abdominal fluid from mice 4 hr after i.a. injection of bacteria. t-Test, n=5 animals per group of N=2 independent experiments. Means and individual values are shown. (**D**) Quantitative assessment of colony forming units in abdominal fluid and (**E**) blood from mice 4 hr after i.a. injection of bacteria. Wilcoxon rank-sum test, n=5 animals per group of N=2 independent experiments. Means and individual values are shown. No growth for controls was detected. (**F**) Kaplan-Meier curves of mice after i.a. injection of bacteria. Log-rank test, n=10 animals per group. (**G**) Heatmap showing surface marker expression (x-axis), which was used to characterize the different immune cell populations (y-axis). (**H**) Concatenated (n=5 animals for each treatment group, n=3 animals for control group of N=2 independent experiments) and down-sampled images of immune cell populations characterized in the abdominal cavity 4 hr after sham treatment or i.a. injection of bacteria. (**I**) Abundance of neutrophils, small peritoneal macrophages (SPM), and CX3CR1pos monocytes in abdominal fluid from mice 4 hr after sham treatment or i.a. injection of bacteria. One-way ANOVA followed by Tukey post hoc test, n=5 animals for each treatment group, n=3 animals for control group of N=2 independent experiments. Means and individual values are shown.

The online version of this article includes the following figure supplement(s) for figure 4:

Figure supplement 1. Immune cell characterization 8 hr after intraabdominal (i.a.) injection of bacteria.

bacteria, we injected ATP-loaded and empty OMV i.a. and investigated the resulting inflammation 1 hr after injection (*Figure 6A*).

In the abdominal fluid, uptake of DiI-stained OMV by leukocytes was independent of ATP cargo (*Figure 6B*, *Figure 6—figure supplement 1*) and all major cell populations with phagocytic ability (LPM, SPM, neutrophils) were highly positive for OMV (*Figure 6—figure supplement 2A and B*). LPM dramatically decreased, whereas neutrophils increased in response to OMV when compared to sham controls (*Figure 6—figure supplement 2C*).
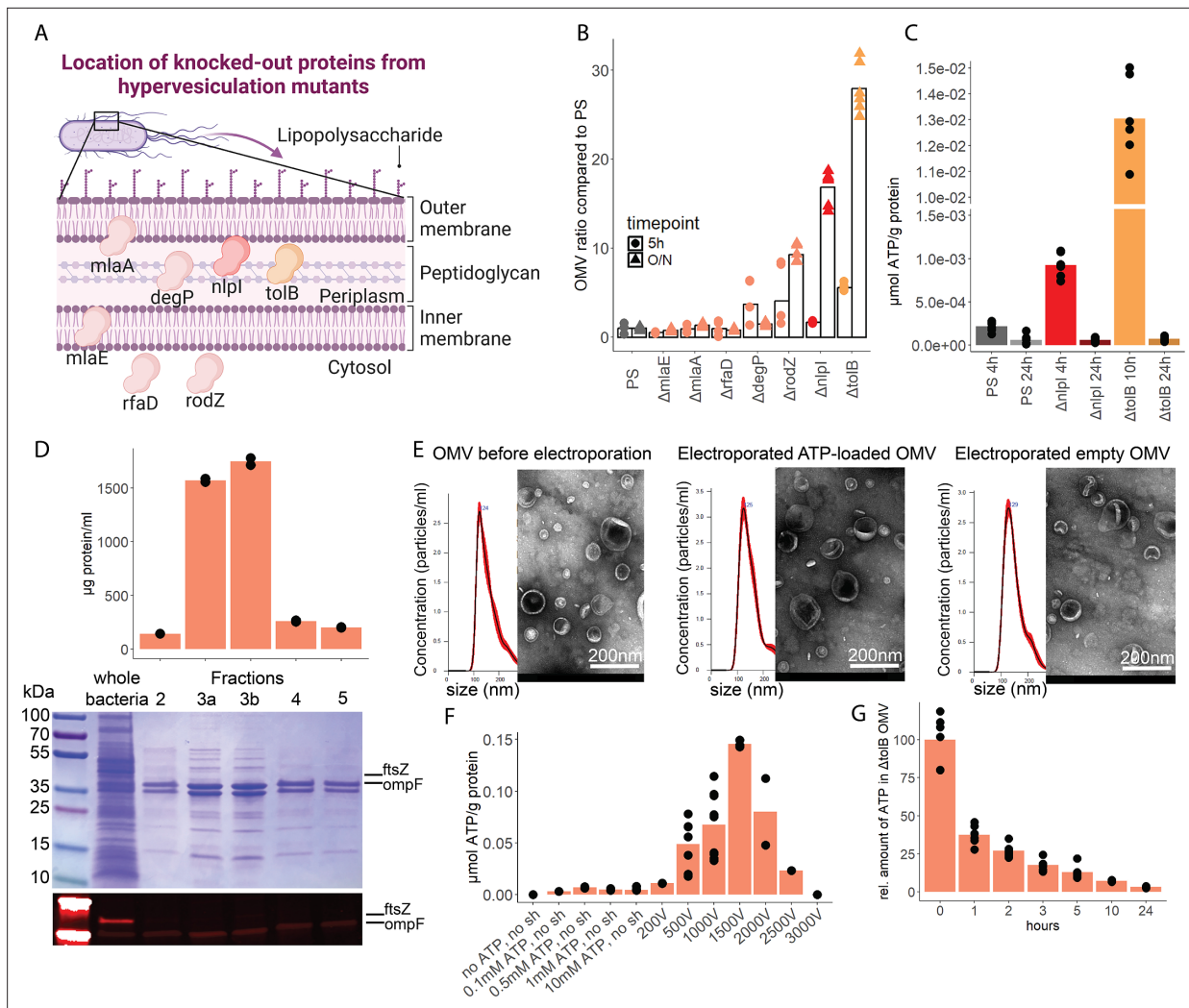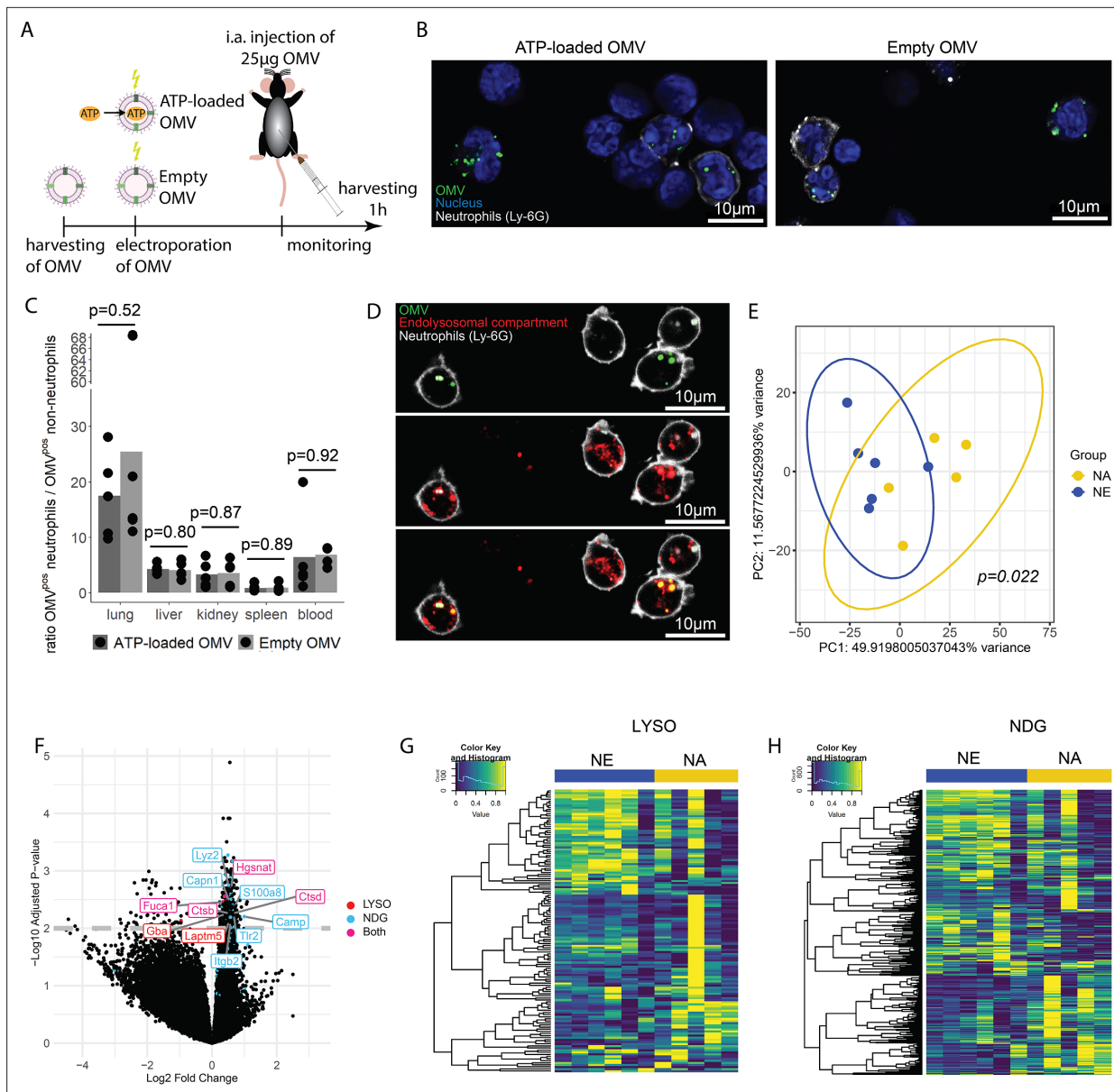
Figure 5. Outer membrane vesicles (OMV) contain adenosine triphosphate (ATP) and can be exploited as a model to assess the systemic relevance of bacterial ATP. (**A**) Illustration depicting the location of assessed proteins that lead to a hypervesiculation phenotype if knocked out in the gram[neg] bacterium *E. coli*. (**B**) Relative amount of OMV compared to the parental strain (PS) isolated from growth cultures of the assessed hypervesiculation mutants after 5 hr (exponential growth phase) and O/N (stationary phase). n=2 measurements of N=3 independent bacteria cultures. Means and individual values are shown. (**C**) Absolute quantification of ATP in OMV isolated from growth cultures of the PS, *ΔnlpI* and *ΔtolB* at their individual peak of ATP release and after 24 hr. n=2 measurements of N=3 independent bacteria cultures. Means and individual values are shown. (**D**) Amount of protein (BCA assay) detected in different fractions after density gradient ultracentrifugation. n=2 measurements of the different fractions. 20 µl of *E. coli* growth culture and 20 µl of each fraction were then characterized by Coomassie blue staining and specific detection of outer membrane ompF and cytoplasmic ftsZ. (**E**) Characterization of OMV by nanoparticle tracking analysis (n=5 measurements per sample) and electron microscopy (representative image) before and after electroporation. (**F**) Absolute quantification of ATP in OMV, which were loaded using different strategies. Columns 2–5: different concentrations of ATP incubated for 1 hr at 37°C (passive filling). Columns 6–12: different voltages with fixed settings for resistance (100 Ω) and capacitance (50 µF). N=2–9 independent experiments. Means and standard deviations are shown. (**G**) Relative quantification of ATP in OMV over 24 hr at 37°C after electroporation (0 hr=100%). n=2 measurements of N=3 independent experiments. Means and individual values are shown.

The online version of this article includes the following figure supplement(s) for figure 5:

Figure supplement 1. Adenosine triphosphate (ATP) measurement of the parental strain (PS), *ΔnlpI* as well as *ΔtolB* and outer membrane vesicle (OMV) collection and characterization.

Figure 6. Bacterial adenosine triphosphate (ATP) within outer membrane vesicles (OMV) upregulates lysosome-related pathways and degranulation processes in neutrophils. (**A**) Experimental approach to determine the systemic role of bacterial ATP in vivo, intraabdominal (i.a.) injecting ATP-loaded or empty OMV. (**B**) Representative microscopic images of cells from the abdominal cavity 1 hr after i.a. injection of either ATP-loaded or empty OMV. OMV: DiI, Nucleus: DAPI, Neutrophils: Ly-6G-FITC. (**C**) Cells from remote organs were isolated 1 hr after i.a. injection of either ATP-loaded or empty OMV. OMV were mainly taken up by neutrophils (except in the spleen, ratio ≈ 1). t-Test with Benjamini-Hochberg correction, n=5 animals per group of N=2 independent experiments. Means and individual values are shown. (**D**) Representative microscopic image of pulmonary neutrophils 1 hr after i.a. injection of either ATP-loaded or empty OMV. OMV co-localize with the endolysosomal compartment. OMV: DiI, Endolysosomal system: LysoTracker Deep Red, Neutrophils: Ly-6G-FITC. (**E**) Pulmonary neutrophils were isolated 1 hr after i.a. injection of ATPγs-loaded or empty OMV, bead-sorted, and RNA sequencing was done. Principal component analysis shows significantly different clustering between neutrophils that took up ATPγs-loaded (NA) or empty OMV (NE). PERMANOVA, n=6 animals in the NE group, n=5 animals in the NA group. Ellipses represent 95% confidence level. (**F**) Volcano plot of RNA sequencing results shows an upregulation of genes mainly in the NA group. Genes classified in either lysosome (LYSO) or neutrophil degranulation pathways (NDG) or both, which were mentioned in the text, were highlighted. (**G**) Heatmap of the lysosome pathway (LYSO) showing the gene expression per sample. (**H**) Heatmap of the neutrophil degranulation pathway (NDG) showing the gene expression per sample.

The online version of this article includes the following figure supplement(s) for figure 6:

Figure supplement 1. Uptake of outer membrane vesicles (OMV) by neutrophils.

Figure supplement 2. Characterization of local immune response in the abdominal cavity.

Figure 6 continued on next page

Within 1 hr, the DiI-stained OMV were distributed throughout the body and mainly taken up by neutrophils, with remarkable differences between organs (*Figure 6—figure supplement 3A and B, C*). The highest ratio of OMV^pos neutrophils compared to all other OMV^pos cells was observed in the lung in an ATP-independent manner (*Figure 6C*). Intracellular fate of engulfed OMV is still a matter of discussion but one possibility is the degradation in the endolysosomal compartment (*Bielaszewska et al., 2017*; *Juodeikis and Carding, 2022*). We therefore injected DiI-stained OMV i.a. to assess to which membrane compartment OMV co-localize. A strong co-localization with the endolysosomal compartment of pulmonary neutrophils was identified (*Figure 6D*).

To determine what pathways OMV-derived bacterial ATP initiates in neutrophils after uptake into the endolysosomal compartment, pulmonary neutrophils were isolated (*Figure 6—figure supplement 4*) for RNA sequencing. Uptake of ATP-loaded OMV resulted in a significantly different transcriptional activity compared to empty OMV (*Figure 6E*): The strongest differences were found in lysosomal and neutrophil degranulation pathways (*Figure 6F*, *Figure 6—figure supplement 5*). In the lysosomal pathway, transcripts for proteins involved in autophagosome-lysosome fusion (Gabarap), endosome to lysosome transport (Hgsnat, Laptm5), or enzymatic cleavage (Capn1, Fuca1, Ctsb, Ctsd, Gba) were significantly higher expressed in response to ATP-loaded OMV when compared to empty OMV (*Figure 6F and G*). Furthermore, neutrophil degranulation was significantly increased in response to ATP-loaded OMV as indicated by increased expression of gene transcripts resulting in antibacterial activity (Lyz2, S100a8, Camp) or NETosis (Tlr2, Itgb2) (*Figure 6F and H*).

In summary, OMV are phagocytosed locally by major cell populations with phagocytic ability. Remotely, OMV were mainly taken up by neutrophils, where they co-localize with the endolysosomal compartment. Delivery of ATP by OMV resulted in an upregulation of lysosomal activation and neutrophil degranulation.

Discussion

In this study, we have demonstrated that ATP release is dependent on the respiratory chain located at the inner bacterial membrane. ATP synthase is most likely dominant compared to cytochrome bo_3 oxidase because of its non-redundant function for ATP generation and bacterial growth. Mutations in one of the cytochrome bo_3 oxidase subunits cyoA, cyoC, or cyoD could be compensated by another subunit. This is supported by lower ATP release in the cyoB mutant, which harbors all three prosthetic groups of the cytochrome bo_3 oxidase and is therefore indispensable for proper function (*Tsubaki et al., 2000*). Alternatively, deficiency in the bo_3-type oxidase could be partially compensated by bd-type oxidases (*Borisov et al., 2011*; *Grauel et al., 2021*).

Instability of the outer bacterial membrane as we have seen for the ΔompF mutant (*Choi and Lee, 2019*) is associated with bacterial death and ATP release. It remains unclear whether loss of ATP results directly in bacterial death or bacterial death is the direct result of impaired outer bacterial membrane stability and ATP release is secondary to bacterial death. However, since the inner membrane and ATP generation remains intact and the periplasmic space is considered generally devoid of ATP, the latter seems more likely (*Kulp and Kuehn, 2010*). Previous studies used Sytox/PI staining and microscopy to identify bacterial death and did not identify bacterial death as a relevant source of extracellular ATP during exponential growth (*Hironaka et al., 2013*). Conversely, we used flow cytometry, a quantitatively more sensitive method, and our data demonstrated that impaired membrane integrity and bacterial death are critical for ATP release during growth. Despite low rates of bacterial death during exponential growth (*Koch, 1959*), and a low ratio of dead to live bacteria, the high gradient between intra- and extracellular ATP (approximately 100–1000× higher) might be sufficient to explain the amount of released ATP measured (*Leduc and van Heijenoort, 1980*; *Mempin et al., 2013*).

ATP was detected within OMV and the concentration of ATP within OMV is sufficient to activate P2-type receptors in lysosomes (*Araujo et al., 2020*; *Junger, 2011*). Furthermore, OMV are released in response to environmental stresses like infection and sepsis (*Kulp and Kuehn, 2010*;

Orench-Rivera and Kuehn, 2016). ATP is likely to activate P2 receptors, which have been shown to be expressed in lysosomes, such as P2X1, P2X3, or P2X4 (*Qureshi et al., 2007*; *Robinson and Murrell-Lagnado, 2013*). OMV can therefore be considered as non-living bacteria-resembling highly inflammatory vesicles (*Jang et al., 2015*; *Kulp and Kuehn, 2010*) that effectively distribute ATP throughout the body to activate cells, such as neutrophils, initiating systemic inflammatory responses. Activation of neutrophils in response to ATP-loaded OMV resulted in upregulation of inflammatory, lysosomal, and neutrophil degranulation pathways as well as an upregulation of the apoptosis pathway and genes involved in NETosis by a hitherto unknown mechanism. These pathways explain in part the low neutrophil counts we observed in mice. Such remote degranulation in response to OMV is unlikely to control bacteria at the source of sepsis but rather harmful to host tissues increasing sepsis severity (*Eichelberger and Goldman, 2020*).

The study has several limitations: Bacterial ATP release is strain specific (*Figure 1*; *Mempin et al., 2013*). As we focused on the laboratory BW25113 *E. coli* strain, it remains to be elucidated if impaired outer membrane integrity and bacterial death are also of such importance in other gram[neg] or also gram[pos] bacteria. The approach to load OMV with ATP is rather artificial; it is, however, the only way to assure that ATP-loaded and empty OMV only differ in their ATP cargo. OMV have surface antigens and contain DNA, proteins, and other metabolites (*Kulp and Kuehn, 2010*), which are known to elicit inflammation as well. This was controlled using the same OMV as baseline vehicles.

Several open questions need to be addressed in future projects: It remains to be determined how OMV are physiologically loaded with ATP. Potentially, despite the lack of a transporter, ATP may similarly to eukaryotic cells leak (*Yegutkin et al., 2006*) across the inner membrane into the periplasmic space that lacks the enzymes for ATP generation. Different types of OMV have been described in recent years, e.g., outer-inner membrane vesicles (O-IMV) or explosive OMV (*Juodeikis and Carding, 2022*; *Takaki et al., 2020*; *Toyofuku et al., 2019*; *Turnbull et al., 2016*; *Turner et al., 2015*), which are composed of outer membrane, inner membrane, and cytoplasmic content. The mechanisms, how these types of OMV are generated, could explain that ATP is found within them. However, the Δ*tolB* mutant produces, unlike other tol mutants, only very few O-IMV (0.1–2% of all OMV) (*Pérez-Cruz et al., 2013*; *Reimer et al., 2021*; *Takaki et al., 2020*) and our western blot analysis suggests that our OMV are primarily outer membrane derived. Future studies may address the ATP cargo of the different OMV subgroups.

OMV are promising diagnostic molecular biomarkers in gram[neg] sepsis (*Michel and Gaborski, 2022*) and it would be of relevance to compare OMV isolated from septic and control patients to assess possible differences in ATP cargo. Furthermore, it remains to be elucidated, which mechanisms lead to low local neutrophil counts. Since ATP is involved in cell death (*Proietti et al., 2019*) as well as in chemotaxis (*Junger, 2011*), increased cell death, impaired infiltration, or a combination of both is possible.

This study reveals that ATP is released by bacteria during growth because of impaired membrane integrity and bacterial death. ATP is also being released via OMV and therefore acts locally (direct release) and systemically (via OMV). Bacterial ATP reduces neutrophil counts, activates the endolysosomal system, and upregulates neutrophil degranulation, which together increase the severity of abdominal infection and early sepsis. These findings have the potential to lead to the development of novel treatments for abdominal sepsis, e.g., by in vitro generated OMV that modulate neutrophil function via delivery of inhibitors to intracellular purinergic receptors during sepsis.

Materials and methods

Human data

From five patients that underwent revision laparotomy because of abdominal sepsis, swabs were taken from abdominal fluid, streaked on LB agar plates (15 g Agar, 5 g Bacto Yeast Extract, 10 g Bacto Tryptone, 5 g NaCl in 1 l ddH$_2$O; Key resources table) and cultivated an/aerobically for 48 hr. The human experimental protocol was approved by the Cantonal Ethics Commission Bern, Switzerland (ethical approval 2017-00573, NCT03554148). Written informed consent was obtained from all patients and the study has been performed in accordance with the Declaration of Helsinki as well as the CONSORT statement.

Mouse handling

Specific pathogen-free C57Bl/6JRccHsd mice (Key resources table) were purchased at the age of 8 weeks from Inotiv (earlier Envigo, the Netherlands) and were housed in ventilated cages in the Central Animal Facility, University of Bern, Switzerland. All experiments were performed in the morning, mice were supplied with a 12 hr light/dark cycle at 22°C and fed ad libitum with chow and water. To minimize cage effects, we mixed mice over several cages and therefore only used female mice. All animal procedures were carried out in accordance with the Swiss guidelines for the care and use of laboratory animals as well as in accordance with the ARRIVE guidelines and were approved by the Animal Care Committee of the Canton of Bern (Switzerland) under the following number: BE41/2022.

CLP sepsis model

To isolate bacteria from mice with abdominal sepsis, CLP was performed as described elsewhere with some minor modifications (*Rittirsch et al., 2009*). In brief, mice were anesthetized s.c. injecting (3 μl/g body weight) a mixture of fentanyl (0.05 mg/ml), dormicum (5 mg/ml), and medetor (1 mg/ml) and were then shaved and disinfected with Betadine. Mid-line laparotomy was performed (approximately 1 cm) and the cecum was exposed. The proximal one third of the cecum was ligated with Vicryl 4-0 (Ethicon, cat# V1224H) and perforated with a 23 G needle. The cecum was returned to the abdominal cavity and the laparotomy was sutured continuously in two layers with prolene 6-0 (Ethicon, cat# MPP8697H). At the end, the antidote (naloxone [0.1 mg/ml], revertor [5 mg/ml], temgesic [0.3 mg/ml]) was s.c. injected (9 μl/g body weight). A semiquantitative score sheet was used to predict animal postoperative well-being. Mice were evaluated every 4 hr according to the following criteria: appearance, level of consciousness, activity, response to stimulus, eye shape, respiratory rate, and respiratory quality and analgesia was applied if necessary. After 10 hr, abdominal fluid was collected, spread on LB agar plates, and cultivated an/aerobically for 48 hr.

Whole 16S-rRNA Sanger sequencing

Twenty-five colonies cultivated from abdominal fluid of patients and mice each described above were randomly picked and collected in separate sterile Eppendorf tubes and resuspended in 1 ml of sterile PBS. Each sample was centrifuged for 5 min at 20,000×g and washed once with 1 ml sterile PBS. The pellet was resuspended in 20 μl of sterile PBS and samples were incubated 5 min at 100°C. 1 μl was used for PCR using GoTaq G2 Green Master Mix (Key resources table) and the following primers (Key resources table) at a final concentration of 0.2 μM:

-fD1: 5'-AGA-GTT-TGA-TCC-TGG-CTC-AG-3'
-fD2: 5'-AGA-GTT-TGA-TCA-TGG-CTC-AG-3'
-rP1: 5'-ACG-GTT-ACC-TTG-TTA-CGA-CTT-3'

PCR conditions were as follows: Initial 5 min at 94°C for denaturation, followed by 35 cycles of 1 min denaturation at 94°C, 1 min annealing at 43°C, and 2 min extension at 72°C, with a final extension for 10 min at 72°C. This resulted in a PCR product of optimally ~1400–1500 bp. 20 μl PCR product were run on 2% agarose gel for 90 min, cut out and purified using QIAquick Gel Extraction Kit (Key resources table). The amplicon concentration was measured using nanodrop (Thermo Fisher Scientific) and Sanger sequencing was done by Microsynth.

Quantification of released bacterial ATP

Bacteria were aerobically grown in 20 ml LB medium (5 g Bacto Yeast Extract, 10 g Bacto Tryptone, 5 g NaCl in 1 l ddH$_2$O; Key resources table) overnight (O/N) (16 hr/37°C/200 rpm) and 0.25 ml of O/N culture were diluted in 100 ml fresh LB medium. Up to 24 hr, 0.25 ml bacteria culture were taken at several time points for growth assessment (OD$_{600}$) and 1 ml was taken for ATP quantification. OD$_{600}$ was measured using a Tecan Spark spectrophotometer. The 1 ml sample for ATP quantification was centrifuged for 5 min at 16,000×g, the supernatant was filtered through a 0.2 μm syringe filter and stored at –80°C. ATP was quantified using a luciferin-luciferase-based assay according to the manufacturer's protocol (ATP Kit SL, Key resources table) and bioluminescence was measured using a Tecan Spark spectrophotometer. In *Figure 3*, LB medium was supplemented with 1 mM calcium or 0.5 mM EDTA for the controls.

Absolute quantification of bacteria and assessment of viability

Growth culture was set up as described above and after 4 hr (ATP peak), samples were taken to quantify bacteria and assess viability. Bacteria were diluted in PBS and stained using the Cell Viability Kit with BD Liquid Counting Beads (Key resources table) according to the manufacturer's protocol. In brief, 100 µl of diluted bacterial growth culture was stained with 1 µl TO dye, 1 µl PI dye, and 10 µl of counting beads were added. The sample was acquired on a CytoFlex S (Beckman Coulter), setting the thresholds for the TO- and the PI-channel to 1000 and analysis was done with FlowJo software (Key resources table). Bacterial biomass was calculated to bacteria/ml culture according to the manufacturer's protocol.

Transformation of *E. coli* PS

The Keio collection (Key resources table) *E. coli* PS was aerobically grown in LB medium O/N (16 hr/37°C/200 rpm). 0.5 ml O/N culture was diluted in 35 ml fresh LB medium and incubated until OD_{600} was 0.35–0.45. Cultures were chilled in ice-water and washed two times with ice-cold 20 ml ultrapure water (Thermo Fisher Scientific, cat# 10977035) (20 min/4°C/3200×g). The supernatant was carefully decanted, and the bacterial pellet was gently resuspended by pipetting (no vortex). After the final wash, the pellet was resuspended in 240 µl ice-cold ultrapure water and kept on ice until EP. 80 µl of ice-cold bacterial cells were mixed with 1 µl plasmid (pBAD28==pEMPTY or pHND10==pAPY, 100–200 ng, Key resources table) in chilled 0.1 cm cuvettes (Bio-Rad, cat# 1652089) and immediately electroporated (voltage = 1.8 kV, capacitance = 25 µF, resistance = 200 Ω). Directly after EP, 1 ml of warm LB medium was added to the cuvette, bacteria were transferred to a tube containing 10 ml pre-warmed LB medium and cultivated for 1 hr at 37°C. Then, bacteria were dispersed on LB agar plates supplemented with ampicillin (100 µg/ml) and incubated at 37°C. The next day, three colonies were picked, streaked on a new ampicillin supplemented LB agar plate, and incubated for 24 hr. The following day, two cryostocks were made from single colonies in LB medium supplemented with 20% glycerol.

Bacteria injection sepsis model

The Keio collection (Key resources table) *E. coli* PS transformed with either pEMPTY or pAPY was aerobically grown O/N (16 hr/37°C/200 rpm) in 20 ml LB medium supplemented with ampicillin (100 µg/ml). PS+pEMPTY and PS+pAPY were washed with PBS (20 min/22°C/3200×g) and resuspended in 20 ml fresh LB medium supplemented with ampicillin (100 µg/ml). To induce the apyrase, L-arabinose (0.03%, Sigma-Aldrich, cat# A3256-25G) was added. After 3 hr, bacteria were washed, resuspended in PBS supplemented with L-arabinose (0.03%) and $2×10^9$ colony forming units were injected i.a. ATP in bacteria cultures and in the abdominal fluid were assessed using the same assay as described above (ATP Kit SL, Key resources table). Mice were evaluated for postoperative well-being every 4 hr as described above. After 4 and 8 hr and when the score reached specific criteria (for the survival experiment), animals were sacrificed using pentobarbital (150 mg/kg body weight) followed by organ collection.

Collection of abdominal fluid, blood, and organs

After pentobarbital injection, the mice were placed on a surgical tray, fixed, the abdomen was shaved, the abdominal skin was disinfected with Betadine and the skin (but not peritoneum) was cut. Abdominal cells were isolated as described elsewhere with some modifications (*Ray and Dittel, 2010*). In brief, a 22 G peripheral IV catheter was inserted into the abdominal cavity through the peritoneum. The abdominal cavity was flushed two times with 5 ml MACS buffer (PBS supplemented with 3% FBS [Gibco, cat# 10500-064], 2% HEPES [Sigma-Aldrich, cat# H0887-100ml], and 2 mM EDTA [Sigma-Aldrich, cat# E5134-500G]). The first 5 ml were used to flush the upper abdomen under pressure, and the second 5 ml, to flush the lower abdomen under pressure. Part of the aspirated fluid was used for aerobic plating, if needed, and the rest was centrifuged for 5 min at 700×g to pellet the abdominal cells for various downstream applications. To collect blood, the peritoneum was opened. 300 µl blood was collected from the inferior vena cava using a 22 G peripheral IV catheter and a 1 ml syringe, which was prefilled with 30 µl 2 mM EDTA. Before organ collection (lungs, liver, kidney, and spleen), the mouse was flushed with 5 ml PBS. Organs were excised and used for downstream processing.

Digestion of organs and preparation of single-cell suspension

Harvested organs were digested (Key resources table; kidney and lungs: 1 mg/ml Col I+1 mg/ml Col IV+1 mg/ml Col D+0.1 mg/ml DNase I in DMEM [Gibco, cat# 31966-047]+3% FBS for 30 min; liver: 1 mg/ml Col IV+0.1 mg/ml DNase I in DMEM+3% FBS for 20 min) at 37°C with a spinning magnet or gently pushed through a 100 μm mesh (spleen). After washing with MACS buffer (5 min/4°C/700×g), erythrocytes were lysed using self-made RBC buffer (90 g NH$_4$Cl, 10 g KHCO$_3$, 370 mg EDTA in 1 l ddH$_2$O for 10× stock). Cells were washed again and stained as described below.

Staining of cells and flow cytometry

First, viability dye (Key resources table) and Fc-block (Key resources table) were diluted in PBS and cells were incubated for 20 min at 4°C in the dark. Cells were washed with MACS buffer and surface staining was done with the listed antibody cocktail:

> (Key resources table: Ly-6G FITC, Ly-6C PerCP-Cy5.5 or Ly-6C PE-Cy7, CD11b APC, CD206 AF700, CD11c APC-eFluor780, CD45 efluor450 or CD45 APC-Cy7, CD19 Super Bright 600, CD3 BV605, NK1.1 BV605, CCR2 BV650, I-A/I-E BV711, CX3CR1 BV785, Siglec F PE, FcεR1α PE/Dazzle 594, CD115 PE-Cy7, F4/80 BUV395)

for 20 min at 4°C in the dark. Cells were washed again and resuspended in MACS buffer for acquisition on an LSR-Fortessa (BD Biosciences). Analysis was done with FlowJo software (Key resources table) and OMIQ web-based analysis platform (https://www.omiq.ai/). To preserve the global structure of abdominal cell populations, uniform manifold approximation and projection was used as dimensionality reduction technique and cell populations were defined using FlowSOM clustering algorithm (*Van Gassen et al., 2015*).

Absolute quantification of bacteria by plating

To count bacteria in isolated abdominal fluid, blood, or growth cultures, serial dilutions were done (1 to 1:100,000) and 50 μl of each dilution was streaked on LB agar plates and aerobically incubated. Plates which had between 20 and 200 colony forming units were used for quantification.

Collection of OMV and ATP measurement of OMV

E. coli PS or hypervesiculation mutants from the Keio collection were grown in LB medium for 5 hr, O/N (16 hr) or 24 hr at 37°C and 200 rpm. Bacteria cultures were then centrifuged (20 min/4°C/3200×g) to pellet bacteria. The supernatant was filtered through a 0.45 μm PES filter (Key resources table) and ultracentrifuged (1.5 hr/4°C/150,000×g) to pellet OMV. When ATP within OMV was measured, OMV were washed in PBS and directly stored at –80°C. ATP was quantified using a luciferin-luciferase-based assay according to the manufacturer's protocol (Microbial ATP Kit HS, Key resources table) and bioluminescence was measured using Tecan Spark spectrophotometer.

If OMV were used for characterization or i.a. injection, first ultracentrifugation was followed by a density gradient ultracentrifugation using OptiPrep (Iodixanol, STEMCELL Technologies, cat# 07820). OMV were resuspended in 50% OptiPrep and OptiPrep gradient (10%, 20%, 30%, 40%, 45%, 50%) was made in underlay technique starting with the 10% layer. Samples were ultracentrifuged (16 hr/4°C/150,000×g) and six fractions (fractions 1, 2, 3a, 3b, 4, and 5) were defined. Fractions were washed separately with PBS (1.5 hr/4°C/150,000×g) and the amount of OMV was determined measuring protein concentration using BCA assay according to the manufacturer's protocol (Thermo Fisher Scientific, cat# 23227). For experiments, only OMV from fraction 3 were used, which were washed with PBS (1.5 hr/4°C/150,000×g), resuspended in PBS, and stored at –80°C until further processing.

EP and staining of OMV

If EP and staining of OMV was performed, OMV were thawed, pelleted (1.5 hr/4°C/150,000×g), the pellet was resuspended in 720 μl EP buffer (500 mM sucrose and 1 ml glycerol in 10 ml ultrapure water) and kept on ice. This suspension was mixed with either 80 μl EP buffer (control) or 80 μl 10 mM ATP (or ATPγs for RNA sequencing experiment) (Key resources table), filled in chilled 0.4 mm EP cuvettes (Bio-Rad, cat# 1652088) and immediately electroporated (voltage = 1100 V, capacitance = 50 μF, resistance = 100 Ω). After EP, the OMV were 1:1 diluted in warm PBS and kept at 37°C for

20 min. DiI (Key resources table) was added 1:100 to the sample during the incubation time. OMV suspension was then washed with PBS (1.5 hr/4°C/150,000×*g*).

OMV injection sepsis model

After the final wash in PBS (see above), OMV were resuspended in NaCl 0.9% and filtered through a 0.45 µm centrifuge filter tube (Sigma-Aldrich, cat# CLS8162-96EA). The final OMV suspension was quantified using a BCA assay. 25 µg of either ATP-loaded OMV or empty OMV were i.a. injected and mice were evaluated as described above. After 1 hr, the animal was sacrificed using pentobarbital followed by organ collection. Tissue digestion and flow cytometry was done as described above.

Assessment of ATP release by OMV

OMV were electroporated as described above. After washing in PBS (1.5 hr/4°C/150,000×*g*), the OMV pellet was resuspended in 6 ml warm PBS and incubated at 37°C. At baseline, after 1, 3, 5, 10, and 24 hr, 1 ml was taken and washed with PBS (1.5 hr/4°C, 150,000×*g*). The OMV pellet was then resuspended in 200 µl PBS to assess protein concentration using a BCA assay, and ATP in OMV was quantified using a luciferin-luciferase-based assay according to the manufacturer's protocol (Intracellular ATP Kit HS, Key resources table). Bioluminescence was measured using a Tecan Spark spectrophotometer.

SDS-PAGE, protein staining, and western blot

20 µl of diluted *E. coli* culture and 20 µl of the different OMV fractions (except fraction 1, since no protein could be detected) were diluted 1:1 with Laemmli/βME (Laemmli buffer solution containing 5% β-mercaptoethanol). The mixture was heated at 100°C for 5 min, shortly centrifuged at 13,000 rpm and loaded on Mini-PROTEAN TGX Gels (Bio-Rad, cat# 4561094). Bio-Rad marker (6 µl) was added to one well and the gel was run at 100 V for 1.5 hr. The gel was then either directly stained with Coomassie blue or transferred to a membrane.

Coomassie blue staining was done as follows: The gel was washed in ddH$_2$O and the staining solution (Coomassie blue 0.1%, 40% ethanol, 10% acetic acid) was heated for 15 s in the microwave. Warm staining solution was added to the gel and gently shaken for 15 min. Then, staining solution was removed, and the gel was washed with ddH$_2$O. Destaining solution (10% ethanol, 7.5% acetic acid) was added for 1 hr, exchanged and left O/N.

To transfer the proteins to a membrane, iBlot2 (Invitrogen) was used. Membranes were then blocked with 4% milk/PBS for 1 hr. FtsZ-antibody (1:200, Key resources table) and ompF-antibody (1:500, Key resources table) were added and incubated O/N at 4°C. The next day, membranes were washed with PBS Tween (PBST, 0.05%) three times for 5 min. Secondary fluorescent antibody was then added in milk (1:10,000, Key resources table) and membrane was incubated for 1 hr. The membrane was washed again with PBST three times for 5 min and then scanned using a Licor Odyssey.

Nanoparticle tracking analysis

Size distribution of OMV was analyzed using the NanoSight NS300 Instrument (Malvern Panalytical, 405 nm laser) according to the manufacturer's protocols. OMV were resuspended in PBS and serial dilutions (1 to 1:100,000) were used to find suitable concentrations. Each experimental sample was analyzed five times. PBS was used to flush the system between the samples and to assess background. For each sample, the relative amount of OMV and the OMV size was recorded, which resulted in a size distribution curve. NTA 2.3 software was used to analyze the data and the following script was used for acquisition (*Gheinani et al., 2018*): SETTEMP 25; CAMERAON; CAMERAGAIN 12; CAMERALEVEL 11; REPEATSTART; SYRINGLOAD 100; DELAY 10; SYRINGSTOP; DELAY 15; CAPTURE 60; DELAY 1; **REPEAT 4**; SETTEMP OFF; PROCESSINGLESETTING; EXPORTRESULTS.

Electron microscopy negative staining

For imaging of negatively stained samples, 5 µl of OMV suspension were adsorbed on glow discharged carbon-coated 400 mesh copper grids (Plano) for 1–5 min. After washing the grids three times by dipping in ultrapure water, the grids were stained with 2% uranyl acetate solution (Electron Microscopy Science) in water for 45 s. The excess fluid was removed by gently pushing the grids sideways onto filter paper. The grids were then examined with an FEI Tecnai Spirit transmission electron microscope at 80 kV, which was equipped with a Veleta TEM CCD camera (Olympus).

Immunofluorescent microscopy

One hour after i.a. injection of DiI-stained OMV, lungs were digested as described above. Single-cell suspension was either fixed and imaged or live cells were imaged. For the fixed approach, single-cell suspension was immunolabeled with FITC-tagged anti-Ly-6G (Key resources table) at 1:100 dilution for 20 min at 4°C in the dark to distinguish neutrophils. Cells were washed once with PBS and applied onto glass slides using Cytospin (Thermo Shandon) for 5 min (1800 rpm). Slides were air-dried for 2 min, washed with PBS, and fixed using 4% paraformaldehyde solution for 10 min. Cell nuclei were stained with DAPI (Key resources table) at 1:5000 concentration in IF buffer (0.25% BSA, 0.1% Triton X-100 in PBS) for 1.5 hr at room temperature in the dark. After washing 3×5 min with IF buffer, the slides were covered and sealed with nail polish.

If live cells were imaged, single-cell suspension was concurrently immunolabeled and stained with Hoechst 33342 (Key resources table) at 1:1000 dilution for cell nuclei, FITC-tagged anti-Ly-6G (Key resources table) at 1:100 dilution for neutrophils and LysoTracker Deep Red (Key resources table) at 1:1000 dilution for lysosomes for 30 min at 37°C in the dark. Cells were washed with MACS buffer and immediately imaged.

Fluorescence images were taken using either a Zeiss LSM710 or a Zeiss LSM980 inverted confocal laser scanning microscope equipped with a ×63 (NA1.4) oil immersion objective. Detector wavelength cutoffs were set to minimize signal crosstalk between fluorophores.

RNA isolation from pulmonary neutrophils

One hour after OMV i.a. injection, lungs were digested as described above. One animal had to be excluded, since the surgical time point has been missed. Neutrophils were isolated from single-cell suspension using Streptavidin MicroBeads (Miltenyi Biotec, cat# 130-048-101) according to the manufacturer's protocol. In brief, cells were counted and incubated with a biotinylated anti-mouse Ly-6G antibody (Key resources table) for 20 min at 4°C. After washing, Streptavidin MicroBeads were added and incubated for 20 min at 4°C. After washing, a MidiMACS separator (Miltenyi Biotec, cat# 130-042-302) together with an LS column (Miltenyi Biotec, cat# 130-042-401) was used to isolate neutrophils and purity of positively selected neutrophils as well as unlabeled cells was assessed by flow cytometry (Key resources table: Ly-6C PE-Cy7, CD11b APC). Neutrophils were pelleted, and supernatant was removed by pipetting. Neutrophils were snap-frozen and stored at –80°C. RNA was isolated directly from frozen neutrophils pellets using Promega ReliaPrep RNA Cell Miniprep System (Key resources table) according to the manufacturer's protocol and quality was assessed using Bioanalyzer and RNA 6000 Nano Kit (RQN 5.8–9.6, median 7.55). Samples were snap-frozen and stored at –80°C until further processing by the Next Generation Sequencing Platform, University of Bern, https://www.ngs.unibe.ch/.

RNA sequencing

RNA sequencing libraries were prepared using Lexogen CORALL total RNA-seq library kit according to the manufacturer's protocol, which includes an rRNA depletion step. Sequencing was performed on an Illumina NovaSeq6000 SP flow cell, 2×50 cycles.

Alignment and quantification

The resulting fastq files were quality controlled using fastqc v0.11.9 (*Babraham Bioinformatics, 2024*). Forward R1 reads were debarcoded by moving the first 12 nucleotides on the 5' end to the name of the read via fastp v0.19.5 (*Chen et al., 2018*). The alignment was performed with STAR v2.7.10a_alpha_220818 (*Dobin et al., 2013*). First, a genome index was generated from the mouse reference genome GRCm39 ENSEMBL v108. Second, the reads were then aligned to the reference using STAR with default parameters. Gene read counts were quantified using featureCounts from subread v2.0.1 using the mm108 GTF annotation with default parameters (*Liao et al., 2014*).

Data visualization

The data from the read count matrix was normalized to reads per million and log-transformed, $x \rightarrow \log(1+x)$. The resulting data was used for principal component analysis, which was performed with the R function *prcomp* and visualized with a custom script using ggplot2 (*Wickham, 2016*).

Differential gene expression

Differentially expressed genes were computed using the R package DESeq2 (*Love et al., 2014*).

Pathway enrichment analysis

The differentially expressed genes obtained from DESeq2 with an adjusted p-value below 0.01 were uploaded to Metascape for pathway analysis on December 5, 2023 (*Zhou et al., 2019*).

Heatmaps

The lists of genes of the pathways of interest were obtained from genome.jp for the KEGG pathways and using the R function *gconvert* from the R package gprofiler2 otherwise (*Kolberg and Raudvere, 2023*). The log-transformed data was used and the heatmaps were done with the heatmap.2 function of the R package gplots with the hierarchical cluster method 'complete' using Pearson's correlation distance (*Warnes et al., 2022*).

Volcano plot

The volcano plots were performed with the R package ggplot2 and a custom R script (*Wickham, 2016*).

Statistical analysis

Descriptive statistics and statistical tests were performed using Prism software (Key resources table) or R and RStudio (Key resources table). For differences between two groups a t-test was applied when data was normally distributed (parametric). Otherwise, a Wilcoxon rank-sum test was used (nonparametric). For differences between more than two groups, a one-way ANOVA followed by a Tukey post hoc test (parametric), or a Kruskal-Wallis test followed by a pairwise Wilcoxon rank-sum test with Benjamini-Hochberg correction (nonparametric) was used. For survival analyses, a log-rank test was used. No one-tailed tests were used. No method was used to predetermine experimental sample sizes. A linear model and the correlation between ATP and OD_{600} in *Figure 2* and *Figure 3* were computed using the R functions *lm* and *cor.test* with the following parameters:

   stats::cor.test($data$variable$ATP, $data$variable$growth, alternative = "two.sided", method = "pearson") summary(stats::lm($variable$ATP ~ $variable$growth, data = $data$)).

   $p < 0.05$ (P==padj, when correction for multiple testing was necessary) was considered significant in all statistical analyses unless stated otherwise in the figure legend. Significant differences are in *italic*.

Acknowledgements

Additional information

Author contributions

Daniel Spari, Conceptualization, Data curation, Software, Formal analysis, Validation, Investigation, Visualization, Methodology, Writing - original draft, Project administration, Writing - review and editing; Annina Schmid, Formal analysis, Investigation, Writing - original draft; Daniel Sanchez-Taltavull, Data curation, Software, Formal analysis, Visualization; Shaira Murugan, Investigation; Keely Keller, Data curation, Software, Writing - original draft; Nadia Ennaciri, Formal analysis, Investigation; Lilian Salm, Investigation, Methodology, Writing - original draft; Deborah Stroka, Resources, Funding acquisition, Methodology, Writing - original draft, Writing - review and editing; Guido Beldi, Conceptualization, Resources, Supervision, Funding acquisition, Methodology, Writing - original draft, Project administration, Writing - review and editing

Author ORCIDs

Daniel Spari ⓘ https://orcid.org/0000-0002-5028-0851
Lilian Salm ⓘ https://orcid.org/0000-0002-6812-3678
Deborah Stroka ⓘ https://orcid.org/0000-0002-3517-3871
Guido Beldi ⓘ https://orcid.org/0000-0002-9914-3807

Ethics

NCT03554148.

The human experimental protocol was approved by the Cantonal Ethics Commission Bern, Switzerland (ethical approval 2017-00573, NCT03554148). Written informed consent was obtained from all patients and the study has been performed in accordance with the Declaration of Helsinki as well as the CONSORT statement.

All animal procedures were carried out in accordance with the Swiss guidelines for the care and use of laboratory animals as well as in accordance with the ARRIVE guidelines and were approved by the Animal Care Committee of the Canton of Bern (Switzerland) under the following number: BE41/2022.

Peer review material

Reviewer #1 (Public review): https://doi.org/10.7554/eLife.96678.3.sa1
Reviewer #2 (Public review): https://doi.org/10.7554/eLife.96678.3.sa2
Author response https://doi.org/10.7554/eLife.96678.3.sa3

Additional files

Supplementary files

• MDAR checklist

Data availability

RNA sequencing data has been deposited in Gene Expression Omnibus (GEO) under the accession code GSE272296. In addition, all raw data, metadata and code are publicly available at BORIS Portal of the University of Bern under a CC-BY licence: https://doi.org/10.48620/418.

The following datasets were generated:

Author(s)	Year	Dataset title	Dataset URL	Database and Identifier
Spari D, Schmid A, Sánchez-Taltavull D, Murugan S, Keller K, Ennaciri N, Salm L, Stroka D, Beldi G	2024	Released Bacterial ATP Shapes Local and Systemic Inflammation during Abdominal Sepsis	https://www.ncbi.nlm.nih.gov/geo/query/acc.cgi?acc=GSE272296	NCBI Gene Expression Omnibus, GSE272296
Beldi G, Keller KA, Sánchez Taltavull D, Murugan S, Schmid AB, Spari D, Ennaciri NS, Salm L, Keogh-Stroka DM	2024	Released Bacterial ATP Shapes Local and Systemic Inflammation during Abdominal Sepsis	https://doi.org/10.48620/418	BORIS Portal, 10.48620/418

References

Alvarez CL, Corradi G, Lauri N, Marginedas-Freixa I, Leal Denis MF, Enrique N, Mate SM, Milesi V, Ostuni MA, Herlax V, Schwarzbaum PJ. 2017. Dynamic regulation of extracellular ATP in *Escherichia coli The Biochemical Journal* **474**:1395–1416. DOI: https://doi.org/10.1042/BCJ20160879, PMID: 28246335

Araujo MEG, Liebscher G, Hess MW, Huber LA. 2020. Lysosomal size matters. *Traffic* **21**:60–75. DOI: https://doi.org/10.1111/tra.12714, PMID: 31808235

Arbizu PM. 2023. pairwiseAdonis cb190f7. GitHub. https://github.com/pmartinezarbizu/pairwiseAdonis

Atarashi K, Nishimura J, Shima T, Umesaki Y, Yamamoto M, Onoue M, Yagita H, Ishii N, Evans R, Honda K, Takeda K. 2008. ATP drives lamina propria T(H)17 cell differentiation. *Nature* **455**:808–812. DOI: https://doi.org/10.1038/nature07240, PMID: 18716618

Baba T, Ara T, Hasegawa M, Takai Y, Okumura Y, Baba M, Datsenko KA, Tomita M, Wanner BL, Mori H. 2006. Construction of *Escherichia coli* K-12 in-frame, single-gene knockout mutants: the Keio collection *Molecular Systems Biology* **2**:2006.0008. DOI: https://doi.org/10.1038/msb4100050, PMID: 16738554

Babraham Bioinformatics. 2024. FastQC A quality control tool for high throughput sequence data. Bioinformatics. http://www.bioinformatics.babraham.ac.uk/projects/fastqc/

Baeza N, Mercade E. 2021. Relationship between membrane vesicles, extracellular ATP and biofilm formation in antarctic gram-negative bacteria. *Microbial Ecology* **81**:645–656. DOI: https://doi.org/10.1007/s00248-020-01614-6, PMID: 33025062

Bielaszewska M, Rüter C, Bauwens A, Greune L, Jarosch KA, Steil D, Zhang W, He X, Lloubes R, Fruth A, Kim KS, Schmidt MA, Dobrindt U, Mellmann A, Karch H. 2017. Host cell interactions of outer membrane vesicle-associated virulence factors of enterohemorrhagic *Escherichia coli* O157: Intracellular delivery, trafficking and mechanisms of cell injury. *PLOS Pathogens* **13**:e1006159. DOI: https://doi.org/10.1371/journal.ppat.1006159, PMID: 28158302

Bittel M, Reichert P, Sarfati I, Dressel A, Leikam S, Uderhardt S, Stolzer I, Phu TA, Ng M, Vu NK, Tenzer S, Distler U, Wirtz S, Rothhammer V, Neurath MF, Raffai RL, Günther C, Momma S. 2021. Visualizing transfer of microbial biomolecules by outer membrane vesicles in microbe-host-communication in vivo. *Journal of Extracellular Vesicles* **10**:e12159. DOI: https://doi.org/10.1002/jev2.12159, PMID: 34664784

Bitto NJ, Chapman R, Pidot S, Costin A, Lo C, Choi J, D'Cruze T, Reynolds EC, Dashper SG, Turnbull L, Whitchurch CB, Stinear TP, Stacey KJ, Ferrero RL. 2017. Bacterial membrane vesicles transport their DNA cargo into host cells. *Scientific Reports* **7**:7072. DOI: https://doi.org/10.1038/s41598-017-07288-4, PMID: 28765539

Borisov VB, Gennis RB, Hemp J, Verkhovsky MI. 2011. The cytochrome bd respiratory oxygen reductases *Biochimica et Biophysica Acta* **1807**:1398–1413. DOI: https://doi.org/10.1016/j.bbabio.2011.06.016, PMID: 21756872

Burnstock G. 2020. Introduction to purinergic signaling. Pelegrín P (Ed). *Purinergic Signaling*. Springer. p. 1–15. DOI: https://doi.org/10.1007/978-1-4939-9717-6_1

Cao M, Wang G, Xie J. 2023. Immune dysregulation in sepsis: experiences, lessons and perspectives. *Cell Death Discovery* **9**:465. DOI: https://doi.org/10.1038/s41420-023-01766-7, PMID: 38114466

Chen S, Zhou Y, Chen Y, Gu J. 2018. fastp: an ultra-fast all-in-one FASTQ preprocessor. *Bioinformatics* **34**:i884–i890. DOI: https://doi.org/10.1093/bioinformatics/bty560, PMID: 30423086

Choi U, Lee CR. 2019. Distinct roles of outer membrane porins in antibiotic resistance and membrane integrity in *Escherichia coli. Frontiers in Microbiology* **10**:953. DOI: https://doi.org/10.3389/fmicb.2019.00953, PMID: 31114568

Diekema DJ, Hsueh PR, Mendes RE, Pfaller MA, Rolston KV, Sader HS, Jones RN. 2019. The microbiology of bloodstream infection: 20-year trends from the SENTRY antimicrobial surveillance program. *Antimicrobial Agents and Chemotherapy* **63**:e00355-19. DOI: https://doi.org/10.1128/AAC.00355-19, PMID: 31010862

Ding Q, Quah SY, Tan KS. 2016a. Secreted adenosine triphosphate from Aggregatibacter actinomycetemcomitans triggers chemokine response. *Molecular Oral Microbiology* **31**:423–434. DOI: https://doi.org/10.1111/omi.12143, PMID: 26470857

Ding Q, Tan KS. 2016b. The danger signal extracellular ATP is an inducer of *Fusobacterium nucleatum* biofilm dispersal. *Frontiers in Cellular and Infection Microbiology* **6**:155. DOI: https://doi.org/10.3389/fcimb.2016.00155, PMID: 27909688

Di Virgilio F, Sarti AC, Coutinho-Silva R. 2020. Purinergic signaling, DAMPs, and inflammation. *American Journal of Physiology. Cell Physiology* **318**:C832–C835. DOI: https://doi.org/10.1152/ajpcell.00053.2020, PMID: 32159362

Dobin A, Davis CA, Schlesinger F, Drenkow J, Zaleski C, Jha S, Batut P, Chaisson M, Gingeras TR. 2013. STAR: ultrafast universal RNA-seq aligner. *Bioinformatics* **29**:15–21. DOI: https://doi.org/10.1093/bioinformatics/bts635, PMID: 23104886

Dosch M, Zindel J, Jebbawi F, Melin N, Sanchez-Taltavull D, Stroka D, Candinas D, Beldi G. 2019. Connexin-43-dependent ATP release mediates macrophage activation during sepsis. *eLife* **8**:e42670. DOI: https://doi.org/10.7554/eLife.42670, PMID: 30735126

Eichelberger KR, Goldman WE. 2020. Manipulating neutrophil degranulation as a bacterial virulence strategy. *PLOS Pathogens* **16**:e1009054. DOI: https://doi.org/10.1371/journal.ppat.1009054, PMID: 33301542

Eltzschig HK, Sitkovsky MV, Robson SC. 2012. Purinergic signaling during inflammation. *The New England Journal of Medicine* **367**:2322–2333. DOI: https://doi.org/10.1056/NEJMra1205750, PMID: 23234515

Fu S, Wang Y, Xia X, Zheng JC. 2020. Exosome engineering: Current progress in cargo loading and targeted delivery. *NanoImpact* **20**:100261. DOI: https://doi.org/10.1016/j.impact.2020.100261

Galber C, Carissimi S, Baracca A, Giorgio V. 2021. The ATP synthase deficiency in human diseases. *Life* **11**:325. DOI: https://doi.org/10.3390/life11040325, PMID: 33917760

Gheinani AH, Vögeli M, Baumgartner U, Vassella E, Draeger A, Burkhard FC, Monastyrskaya K. 2018. Improved isolation strategies to increase the yield and purity of human urinary exosomes for biomarker discovery. *Scientific Reports* **8**:3945. DOI: https://doi.org/10.1038/s41598-018-22142-x, PMID: 29500443

Ghosn EEB, Cassado AA, Govoni GR, Fukuhara T, Yang Y, Monack DM, Bortoluci KR, Almeida SR, Herzenberg LA, Herzenberg LA. 2010. Two physically, functionally, and developmentally distinct peritoneal macrophage subsets. *PNAS* **107**:2568–2573. DOI: https://doi.org/10.1073/pnas.0915000107, PMID: 20133793

Grauel A, Kägi J, Rasmussen T, Makarchuk I, Oppermann S, Moumbock AFA, Wohlwend D, Müller R, Melin F, Günther S, Hellwig P, Böttcher B, Friedrich T. 2021. Structure of *Escherichia coli* cytochrome bd-II type oxidase with bound aurachin D. *Nature Communications* **12**:6498. DOI: https://doi.org/10.1038/s41467-021-26835-2, PMID: 34764272

Hironaka I, Iwase T, Sugimoto S, Okuda K, Tajima A, Yanaga K, Mizunoe Y. 2013. Glucose triggers ATP secretion from bacteria in a growth-phase-dependent manner. *Applied and Environmental Microbiology* **79**:2328–2335. DOI: https://doi.org/10.1128/AEM.03871-12, PMID: 23354720

Ihssen J, Jovanovic N, Sirec T, Spitz U. 2021. Real-time monitoring of extracellular ATP in bacterial cultures using thermostable luciferase. *PLOS ONE* **16**:e0244200. DOI: https://doi.org/10.1371/journal.pone.0244200, PMID: 33481792

Ivancic V, Mastali M, Percy N, Gornbein J, Babbitt JT, Li Y, Landaw EM, Bruckner DA, Churchill BM, Haake DA. 2008. Rapid antimicrobial susceptibility determination of uropathogens in clinical urine specimens by use of ATP bioluminescence. *Journal of Clinical Microbiology* **46**:1213–1219. DOI: https://doi.org/10.1128/JCM.02036-07, PMID: 18272708

Iwase T, Shinji H, Tajima A, Sato F, Tamura T, Iwamoto T, Yoneda M, Mizunoe Y. 2010. Isolation and identification of ATP-secreting bacteria from mice and humans. *Journal of Clinical Microbiology* **48**:1949–1951. DOI: https://doi.org/10.1128/JCM.01941-09, PMID: 20305009

Jang SC, Kim SR, Yoon YJ, Park KS, Kim JH, Lee J, Kim OY, Choi EJ, Kim DK, Choi DS, Kim YK, Park J, Di Vizio D, Gho YS. 2015. In vivo kinetic biodistribution of nano-sized outer membrane vesicles derived from bacteria. *Small* **11**:456–461. DOI: https://doi.org/10.1002/smll.201401803, PMID: 25196673

Junger WG. 2011. Immune cell regulation by autocrine purinergic signalling. *Nature Reviews. Immunology* **11**:201–212. DOI: https://doi.org/10.1038/nri2938, PMID: 21331080

Juodeikis R, Carding SR. 2022. Outer membrane vesicles: Biogenesis, functions, and issues. *Microbiology and Molecular Biology Reviews* **86**:e0003222. DOI: https://doi.org/10.1128/mmbr.00032-22, PMID: 36154136

Kassambara A. 2023. Rstatix: pipe-friendly framework for basic statistical tests. 0.7.2. R Packages. https://cran.r-project.org/web/packages/rstatix/index.html

Kim JH, Yoon YJ, Lee J, Choi EJ, Yi N, Park KS, Park J, Lötvall J, Kim YK, Gho YS. 2013. Outer membrane vesicles derived from *Escherichia coli* up-regulate expression of endothelial cell adhesion molecules in vitro and in vivo. *PLOS ONE* **8**:e59276. DOI: https://doi.org/10.1371/journal.pone.0059276, PMID: 23516621

Koch AL. 1959. Death of bacteria in growing culture. *Journal of Bacteriology* **77**:623–629. DOI: https://doi.org/10.1128/jb.77.5.623-629.1959, PMID: 13654228

Kolberg L, Raudvere U. 2023. Gprofiler2: interface to the "g:profiler" toolset. 0.2.2. R Packages. https://cran.r-project.org/web/packages/gprofiler2/index.html

Kulp A, Kuehn MJ. 2010. Biological functions and biogenesis of secreted bacterial outer membrane vesicles. *Annual Review of Microbiology* **64**:163–184. DOI: https://doi.org/10.1146/annurev.micro.091208.073413, PMID: 20825345

Ledderose C, Bao Y, Kondo Y, Fakhari M, Slubowski C, Zhang J, Junger WG. 2016. Purinergic signaling and the immune response in sepsis: A review. *Clinical Therapeutics* **38**:1054–1065. DOI: https://doi.org/10.1016/j.clinthera.2016.04.002, PMID: 27156007

Leduc M, van Heijenoort J. 1980. Autolysis of *Escherichia coli*. *Journal of Bacteriology* **142**:52–59. DOI: https://doi.org/10.1128/jb.142.1.52-59.1980, PMID: 6768717

Lee EY, Bang JY, Park GW, Choi DS, Kang JS, Kim HJ, Park KS, Lee JO, Kim YK, Kwon KH, Kim KP, Gho YS. 2007. Global proteomic profiling of native outer membrane vesicles derived from *Escherichia coli*. PROTEOMICS **7**:3143–3153. DOI: https://doi.org/10.1002/pmic.200700196, PMID: 17787032

Lee J, Yoon YJ, Kim JH, Dinh NTH, Go G, Tae S, Park KS, Park HT, Lee C, Roh TY, Di Vizio D, Gho YS. 2018. Outer membrane vesicles derived from *Escherichia coli* regulate neutrophil migration by induction of endothelial IL-8. *Frontiers in Microbiology* **9**:2268. DOI: https://doi.org/10.3389/fmicb.2018.02268, PMID: 30369908

Leive L. 1968. Studies on the permeability change produced in coliform bacteria by ethylenediaminetetraacetate. *The Journal of Biological Chemistry* **243**:2373–2380. DOI: https://doi.org/10.1016/S0021-92581893484-8, PMID: 4967584

Lennaárd AJ, Mamand DR, Wiklander RJ, El Andaloussi S, Wiklander OPB. 2021. Optimised electroporation for loading of extracellular vesicles with doxorubicin. *Pharmaceutics* **14**:38. DOI: https://doi.org/10.3390/pharmaceutics14010038, PMID: 35056933

Liao Y, Smyth GK, Shi W. 2014. featureCounts: an efficient general purpose program for assigning sequence reads to genomic features. *Bioinformatics* **30**:923–930. DOI: https://doi.org/10.1093/bioinformatics/btt656

Love MI, Huber W, Anders S. 2014. Moderated estimation of fold change and dispersion for RNA-seq data with DESeq2. *Genome Biology* **15**:550. DOI: https://doi.org/10.1186/s13059-014-0550-8, PMID: 25516281

Lundin A. 2000 Use of firefly luciferase in atp-related assays of biomass, enzymes, and metabolites Lundin A (Ed). *Methods in Enzymology*. Elsevier. p. 346–370. DOI: https://doi.org/10.1016/S0076-6879(00)05499-9

McBroom AJ, Johnson AP, Vemulapalli S, Kuehn MJ. 2006. Outer membrane vesicle production by *Escherichia coli* is independent of membrane instability. *Journal of Bacteriology* **188**:5385–5392. DOI: https://doi.org/10.1128/JB.00498-06, PMID: 16855227

Mempin R, Tran H, Chen C, Gong H, Kim Ho K, Lu S. 2013. Release of extracellular ATP by bacteria during growth. *BMC Microbiology* **13**:301. DOI: https://doi.org/10.1186/1471-2180-13-301, PMID: 24364860

Michel LV, Gaborski T. 2022. Outer membrane vesicles as molecular biomarkers for Gram-negative sepsis: Taking advantage of nature's perfect packages. *The Journal of Biological Chemistry* **298**:102483. DOI: https://doi.org/10.1016/j.jbc.2022.102483, PMID: 36108741

Mureşan MG, Balmoş IA, Badea I, Santini A. 2018. Abdominal sepsis: An update. *The Journal of Critical Care Medicine* **4**:120–125. DOI: https://doi.org/10.2478/jccm-2018-0023

Oksanen J, Simpson GL, Blanchet FG, Kindt R, Legendre P, Minchin PR, O'Hara RB, Solymos P, Stevens MHH, Szoecs E, Wagner H, Barbour M, Bedward M, Bolker B, Borcard D, Carvalho G, Chirico M, Caceres MD, Durand S, Weedon J. 2022. Vegan: community ecology package. 2.6-4. R Packages. https://cran.r-project.org/web/packages/vegan/index.html

Orench-Rivera N, Kuehn MJ. 2016. Environmentally controlled bacterial vesicle-mediated export. *Cellular Microbiology* **18**:1525–1536. DOI: https://doi.org/10.1111/cmi.12676, PMID: 27673272

Park KS, Choi KH, Kim YS, Hong BS, Kim OY, Kim JH, Yoon CM, Koh GY, Kim YK, Gho YS. 2010. Outer membrane vesicles derived from *Escherichia coli* induce systemic inflammatory response syndrome. *PLOS ONE* **5**:e11334. DOI: https://doi.org/10.1371/journal.pone.0011334, PMID: 20596524

Park KS, Lee J, Jang SC, Kim SR, Jang MH, Lötvall J, Kim YK, Gho YS. 2013. Pulmonary inflammation induced by bacteria-free outer membrane vesicles from *Pseudomonas aeruginosa*. *American Journal of Respiratory Cell and Molecular Biology* **49**:637–645. DOI: https://doi.org/10.1165/rcmb.2012-0370OC, PMID: 23713467

Pérez-Cruz C, Carrión O, Delgado L, Martinez G, López-Iglesias C, Mercade E. 2013. New type of outer membrane vesicle produced by the Gram-negative bacterium Shewanella vesiculosa M7T: implications for DNA content. *Applied and Environmental Microbiology* **79**:1874–1881. DOI: https://doi.org/10.1128/AEM.03657-12, PMID: 23315742

Pérez-Cruz C, Delgado L, López-Iglesias C, Mercade E. 2015. Outer-inner membrane vesicles naturally secreted by gram-negative pathogenic bacteria. *PLOS ONE* **10**:e0116896. DOI: https://doi.org/10.1371/journal.pone.0116896, PMID: 25581302

Perruzza L, Gargari G, Proietti M, Fosso B, D'Erchia AM, Faliti CE, Rezzonico-Jost T, Scribano D, Mauri L, Colombo D, Pellegrini G, Moregola A, Mooser C, Pesole G, Nicoletti M, Norata GD, Geuking MB, McCoy KD, Guglielmetti S, Grassi F. 2017. T follicular helper cells promote a beneficial gut ecosystem for host metabolic homeostasis by sensing microbiota-derived extracellular ATP. *Cell Reports* **18**:2566–2575. DOI: https://doi.org/10.1016/j.celrep.2017.02.061, PMID: 28297661

Proietti M, Perruzza L, Scribano D, Pellegrini G, D'Antuono R, Strati F, Raffaelli M, Gonzalez SF, Thelen M, Hardt WD, Slack E, Nicoletti M, Grassi F. 2019. ATP released by intestinal bacteria limits the generation of protective IgA against enteropathogens. *Nature Communications* **10**:250. DOI: https://doi.org/10.1038/s41467-018-08156-z, PMID: 30651557

Qureshi OS, Paramasivam A, Yu JCH, Murrell-Lagnado RD. 2007. Regulation of P2X4 receptors by lysosomal targeting, glycan protection and exocytosis. *Journal of Cell Science* **120**:3838–3849. DOI: https://doi.org/10.1242/jcs.010348, PMID: 17940064

Ray A, Dittel BN. 2010. Isolation of mouse peritoneal cavity cells. *Journal of Visualized Experiments* **35**:1488. DOI: https://doi.org/10.3791/1488, PMID: 20110936

Reimer SL, Beniac DR, Hiebert SL, Booth TF, Chong PM, Westmacott GR, Zhanel GG, Bay DC. 2021. Comparative analysis of outer membrane vesicle isolation methods with an *Escherichia coli* tolA mutant reveals a hypervesiculating phenotype with outer-inner membrane vesicle content. *Frontiers in Microbiology* **12**:628801. DOI: https://doi.org/10.3389/fmicb.2021.628801, PMID: 33746922

Reinhart K, Daniels R, Kissoon N, Machado FR, Schachter RD, Finfer S. 2017. Recognizing sepsis as a global health priority - A WHO resolution. *The New England Journal of Medicine* **377**:414–417. DOI: https://doi.org/10.1056/NEJMp1707170, PMID: 28658587

Rittirsch D, Huber-Lang MS, Flierl MA, Ward PA. 2009. Immunodesign of experimental sepsis by cecal ligation and puncture. *Nature Protocols* **4**:31–36. DOI: https://doi.org/10.1038/nprot.2008.214, PMID: 19131954

Robinson LE, Murrell-Lagnado RD. 2013. The trafficking and targeting of P2X receptors. *Frontiers in Cellular Neuroscience* **7**:233. DOI: https://doi.org/10.3389/fncel.2013.00233, PMID: 24319412

Ross N, Rudis B, Filipovic-Pierucci A, Galili C, Greenwell C. 2021. sjmgarnier/viridis: viridis 0.6.0 (pre-CRAN release). v0.6.0pre. Zenodo. https://doi.org/10.5281/zenodo.4679424

Rudd KE, Johnson SC, Agesa KM, Shackelford KA, Tsoi D, Kievlan DR, Colombara DV, Ikuta KS, Kissoon N, Finfer S, Fleischmann-Struzek C, Machado FR, Reinhart KK, Rowan K, Seymour CW, Watson RS, West TE, Marinho F, Hay SI, Lozano R, et al. 2020. Global, regional, and national sepsis incidence and mortality, 1990–2017: analysis for the Global Burden of Disease Study. *The Lancet* **395**:200–211. DOI: https://doi.org/10.1016/S0140-6736(19)32989-7, PMID: 31911147

Salm L, Shim R, Noskovicova N, Kubes P. 2023. Gata6+ large peritoneal macrophages: an evolutionarily conserved sentinel and effector system for infection and injury. *Trends in Immunology* **44**:129–145. DOI: https://doi.org/10.1016/j.it.2022.12.002, PMID: 36623953

Santapaola D, Del Chierico F, Petrucca A, Uzzau S, Casalino M, Colonna B, Sessa R, Berlutti F, Nicoletti M. 2006. Apyrase, the product of the virulence plasmid-encoded phoN2 (apy) gene of Shigella flexneri, is necessary for proper unipolar IcsA localization and for efficient intercellular spread. *Journal of Bacteriology* **188**:1620–1627. DOI: https://doi.org/10.1128/JB.188.4.1620-1627.2006, PMID: 16452446

Schwechheimer C, Kuehn MJ. 2015. Outer-membrane vesicles from Gram-negative bacteria: biogenesis and functions. *Nature Reviews. Microbiology* **13**:605–619. DOI: https://doi.org/10.1038/nrmicro3525, PMID: 26373371

Scribano D, Petrucca A, Pompili M, Ambrosi C, Bruni E, Zagaglia C, Prosseda G, Nencioni L, Casalino M, Polticelli F, Nicoletti M. 2014. Polar localization of PhoN2, a periplasmic virulence-associated factor of Shigella flexneri, is required for proper IcsA exposition at the old bacterial pole. *PLOS ONE* **9**:e90230. DOI: https://doi.org/10.1371/journal.pone.0090230, PMID: 24587292

Slowikowski K, Schep A, Hughes S, Dang TK, Lukauskas S, Irisson JO, Kamvar ZN, Ryan T, Christophe D, Hiroaki Y, Gramme P, Abdol AM, Barrett M, Cannoodt R, Krassowski M, Chirico M, Aphalo P, Barton F. 2023. Ggrepel: automatically position non-overlapping text labels with "ggplot2." 0.9.5. R Packages. https://cran.r-project.org/web/packages/ggrepel/index.html

Spari D, Beldi G. 2020. Extracellular ATP as an inter-kingdom signaling molecule: Release Mechanisms by bacteria and its implication on the host. *International Journal of Molecular Sciences* **21**:5590. DOI: https://doi.org/10.3390/ijms21155590, PMID: 32759857

Takaki K, Tahara YO, Nakamichi N, Hasegawa Y, Shintani M, Ohkuma M, Miyata M, Futamata H, Tashiro Y. 2020. Multilamellar and multivesicular outer membrane vesicles produced by a buttiauxella agrestis *tolB* Mutant. *Applied and Environmental Microbiology* **86**:e01131-20. DOI: https://doi.org/10.1128/AEM.01131-20, PMID: 32801184

Toyofuku M, Nomura N, Eberl L. 2019. Types and origins of bacterial membrane vesicles. *Nature Reviews. Microbiology* **17**:13–24. DOI: https://doi.org/10.1038/s41579-018-0112-2, PMID: 30397270

Tsubaki M, Hori H, Mogi T. 2000. Probing molecular structure of dioxygen reduction site of bacterial quinol oxidases through ligand binding to the redox metal centers. *Journal of Inorganic Biochemistry* **82**:19–25. DOI: https://doi.org/10.1016/s0162-0134(00)00140-9, PMID: 11132627

Turnbull L, Toyofuku M, Hynen AL, Kurosawa M, Pessi G, Petty NK, Osvath SR, Cárcamo-Oyarce G, Gloag ES, Shimoni R, Omasits U, Ito S, Yap X, Monahan LG, Cavaliere R, Ahrens CH, Charles IG, Nomura N, Eberl L, Whitchurch CB. 2016. Explosive cell lysis as a mechanism for the biogenesis of bacterial membrane vesicles and biofilms. *Nature Communications* **7**:11220. DOI: https://doi.org/10.1038/ncomms11220, PMID: 27075392

Turner L, Praszkier J, Hutton ML, Steer D, Ramm G, Kaparakis-Liaskos M, Ferrero RL. 2015. Increased outer membrane vesicle formation in a *Helicobacter pylori* tolB mutant. *Helicobacter* **20**:269–283. DOI: https://doi.org/10.1111/hel.12196, PMID: 25669590

Van Gassen S, Callebaut B, Van Helden MJ, Lambrecht BN, Demeester P, Dhaene T, Saeys Y. 2015. FlowSOM: Using self-organizing maps for visualization and interpretation of cytometry data. *Cytometry. Part A* **87**:636–645. DOI: https://doi.org/10.1002/cyto.a.22625, PMID: 25573116

Vega-Pérez A, Villarrubia LH, Godio C, Gutiérrez-González A, Feo-Lucas L, Ferriz M, Martínez-Puente N, Alcaín J, Mora A, Sabio G, López-Bravo M, Ardavín C. 2021. Resident macrophage-dependent immune cell scaffolds drive anti-bacterial defense in the peritoneal cavity. *Immunity* **54**:2578–2594. DOI: https://doi.org/10.1016/j.immuni.2021.10.007, PMID: 34717795

Warnes GR, Bolker B, Bonebakker L, Gentleman R, Huber W, Liaw A, Lumley T, Maechler M, Magnusson A, Moeller S, Schwartz M, Venables B, Galili T. 2022. Gplots: various R programming tools for plotting data. 3.1.3. R Packages. https://cran-r-project.org/web/packages/gplots/index.html

Weisburg WG, Barns SM, Pelletier DA, Lane DJ. 1991. 16S ribosomal DNA amplification for phylogenetic study. *Journal of Bacteriology* **173**:697–703. DOI: https://doi.org/10.1128/jb.173.2.697-703.1991, PMID: 1987160

Wickham H. 2016. *Ggplot2*. Springer International Publishing. DOI: https://doi.org/10.1007/978-3-319-24277-4

Wickham H, Bryan J. 2023a. readxl: Read Excel Files 1.4.3. R Packages. https://cran-r-project.org/web/packages/readxl/index.html

Wickham H, François R, Henry L, Müller K. 2023b. Dplyr: A grammar of data manipulation. 1.1.4. R Packages. https://cran.r-project.org/web/packages/dplyr/index.html

Xu S, Chen M, Feng T, Zhan L, Zhou L, Yu G. 2021. Use *ggbreak* to effectively utilize plotting space to deal with large datasets and outliers. *Frontiers in Genetics* **12**:774846. DOI: https://doi.org/10.3389/fgene.2021.774846, PMID: 34795698

Yamamoto N, Nakahigashi K, Nakamichi T, Yoshino M, Takai Y, Touda Y, Furubayashi A, Kinjyo S, Dose H, Hasegawa M, Datsenko KA, Nakayashiki T, Tomita M, Wanner BL, Mori H. 2009. Update on the Keio collection of *Escherichia coli* single-gene deletion mutants. *Molecular Systems Biology* **5**:335. DOI: https://doi.org/10.1038/msb.2009.92, PMID: 20029369

Yegutkin GG, Mikhailov A, Samburski SS, Jalkanen S. 2006. The detection of micromolar pericellular ATP pool on lymphocyte surface by using lymphoid ecto-adenylate kinase as intrinsic ATP sensor. *Molecular Biology of the Cell* **17**:3378–3385. DOI: https://doi.org/10.1091/mbc.e05-10-0993, PMID: 16707571

Zhou Y, Zhou B, Pache L, Chang M, Khodabakhshi AH, Tanaseichuk O, Benner C, Chanda SK. 2019. Metascape provides a biologist-oriented resource for the analysis of systems-level datasets. *Nature Communications* **10**:1523. DOI: https://doi.org/10.1038/s41467-019-09234-6, PMID: 30944313

Zindel J, Peiseler M, Hossain M, Deppermann C, Lee WY, Haenni B, Zuber B, Deniset JF, Surewaard BGJ, Candinas D, Kubes P. 2021. Primordial GATA6 macrophages function as extravascular platelets in sterile injury. *Science* **371**:eabe0595. DOI: https://doi.org/10.1126/science.abe0595, PMID: 33674464

Appendix 1

Appendix 1—key resources table

Reagent type (species) or resource	Designation	Source or reference	Identifiers	Additional information
Strain, strain background (*Mus musculus, female*)	Wild-type mice	Inotiv, the Netherlands	C57Bl/6JRccHsd	
Strain, strain background (*Enterococcus faecalis*)	Iso1	This paper	*NA*	See Materials and methods: Human data
Strain, strain background (*Escherichia coli*)	Iso2	This paper	*NA*	See Materials and methods: Human data
Strain, strain background (*Klebsiella pneumoniae*)	Iso3	This paper	*NA*	See Materials and methods: Human data
Strain, strain background (*Staphylococcus aureus*)	Iso4	This paper	*NA*	See Materials and methods: Human data
Strain, strain background (*E. faecalis*)	Iso5	This paper	*NA*	See Materials and methods: CLP sepsis model
Strain, strain background (*E. coli*)	Iso6	This paper	*NA*	See Materials and methods: CLP sepsis model
Strain, strain background (*S. aureus*)	Iso7	This paper	*NA*	See Materials and methods: CLP sepsis model
Strain, strain background (*E. coli*)	Parental strain (PS)	Keio collection; *Baba et al., 2006*	BW25113	
Strain, strain background (*E. coli*)	ΔcyoA	Keio collection; *Baba et al., 2006*	JW0422-1	See *Figure 2*
Strain, strain background (*E. coli*)	ΔcyoB	Keio collection; *Baba et al., 2006*	JW0421-1	See *Figure 2*
Strain, strain background (*E. coli*)	ΔcyoC	Keio collection; *Baba et al., 2006*	JW0420-1	See *Figure 2*
Strain, strain background (*E. coli*)	ΔcyoD	Keio collection; *Baba et al., 2006*	JW0419-1	See *Figure 2*
Strain, strain background (*E. coli*)	ΔatpA	Keio collection; *Baba et al., 2006*	JW3712-1	See *Figure 2*
Strain, strain background (*E. coli*)	ΔatpB	Keio collection; *Baba et al., 2006*	JW3716-1	See *Figure 2*
Strain, strain background (*E. coli*)	ΔatpC	Keio collection; *Baba et al., 2006*	JW3709-2	See *Figure 2*
Strain, strain background (*E. coli*)	ΔatpD	Keio collection; *Baba et al., 2006*	JW3710-1	See *Figure 2*
Strain, strain background (*E. coli*)	ΔatpE	Keio collection; *Baba et al., 2006*	JW3715-1	See *Figure 2*
Strain, strain background (*E. coli*)	ΔatpF	Keio collection; *Baba et al., 2006*	JW3714-2	See *Figure 2*
Strain, strain background (*E. coli*)	ΔatpH	Keio collection; *Baba et al., 2006*	JW3713-1	See *Figure 2*
Strain, strain background (*E. coli*)	ΔompF	Keio collection; *Baba et al., 2006*	JW0912-1	See *Figure 3*
Strain, strain background (*E. coli*)	ΔompC	Keio collection; *Baba et al., 2006*	JW2203-1	See *Figure 3*

Appendix 1 Continued on next page

Appendix 1 Continued

Reagent type (species) or resource	Designation	Source or reference	Identifiers	Additional information
Strain, strain background (*E. coli*)	Δ*lamB*	Keio collection; *Baba et al., 2006*	JW3996-1	See *Figure 3*
Strain, strain background (*E. coli*)	Δ*phoE*	Keio collection; *Baba et al., 2006*	JW0231-1	See *Figure 3*
Strain, strain background (*E. coli*)	Δ*mlaA*	Keio collection; *Baba et al., 2006*	JW2343-1	See *Figure 5*
Strain, strain background (*E. coli*)	Δ*mlaE*	Keio collection; *Baba et al., 2006*	JW3161-1	See *Figure 5*
Strain, strain background (*E. coli*)	Δ*nlpI*	Keio collection; *Baba et al., 2006*	JW3132-1	See *Figure 5*
Strain, strain background (*E. coli*)	Δ*tolB*	Keio collection; *Baba et al., 2006*	JW5100-1	See *Figure 5*
Strain, strain background (*E. coli*)	Δ*degP*	Keio collection; *Baba et al., 2006*	JW0157-1	See *Figure 5*
Strain, strain background (*E. coli*)	Δ*rfaD*	Keio collection; *Baba et al., 2006*	JW3594-1	See *Figure 5*
Strain, strain background (*E. coli*)	Δ*rodZ*	Keio collection; *Baba et al., 2006*	JW2500-1	See *Figure 5*
Antibody	Purified anti-Ms CD16/32, monoclonal	BioLegend	Cat# 101302; clone 93; Lot# B298973; RRID: AB_312801	(1:200)
Antibody	Rat anti-Ms Ly-6G (FITC), monoclonal	BD Biosciences	Cat# 551460; clone 1A8; Lot# 9068981; RRID: AB_394207	(1:100)
Antibody	Rat anti-Ms Ly-6C (PerCP-Cyanine5.5), monoclonal	Thermo Fisher Scientific	Cat# 45-5932-82; clone HK1.4; Lot# 2309273; RRID: AB_2723343	(1:100)
Antibody	Rat anti-Ms/Hs CD11b (APC), monoclonal	BioLegend	Cat# 101212; clone M1/70; Lot# B312600; RRID: AB_312795	(1:800)
Antibody	Rat anti-Ms CD206 (AF700), monoclonal	BioLegend	Cat# 141733; clone C068C2; Lot# B278058; RRID: AB_2629636	(1:300)
Antibody	Armenian hamster anti-Ms CD11c (APC-eFluor780), monoclonal	Thermo Fisher Scientific	Cat# 47-0114-80; clone N418; Lot# 2133269; RRID: AB_1548652	(1:300)
Antibody	Rat anti-Ms CD45 (efluor450), monoclonal	Thermo Fisher Scientific	Cat# 48-0451-82; clone 30-F11; Lot# 2005853 RRID: AB_1518806	(1:600)
Antibody	Rat anti-Ms CD19 (Super Bright 600), monoclonal	Thermo Fisher Scientific	Cat# 63-0193-82; clone eBio1D3; Lot# 2366423; RRID: AB_2637308	(1:150)
Antibody	Rat anti-Ms CD3 (BV 605), monoclonal	BioLegend	Cat# 100237; clone 17A2; Lot# B389899; RRID: AB_2562039	(1:100)
Antibody	Mouse anti-Ms NK1.1 (BV605), monoclonal	BioLegend	Cat# 108739; clone PK-136; Lot# B389899; RRID: AB_2562273	(1:150)
Antibody	Rat anti-Ms CCR2 (BV650), monoclonal	BioLegend	Cat# 150613; clone SA203G11; Lot# B294599; RRID: AB_2721553	(1:100)
Antibody	Rat anti-Ms I-A/I-E (BV711), monoclonal	BioLegend	Cat# 107643; clone M5/114.15.2; Lot# B299330; RRID: AB_2565976	(1:600)

Appendix 1 Continued

Reagent type (species) or resource	Designation	Source or reference	Identifiers	Additional information
Antibody	Mouse anti-Ms CX3CR1 (BV785), monoclonal	BioLegend	Cat# 149029; clone SA011F11; Lot# B304744; RRID: AB_2565938	(1:300)
Antibody	Rat anti-Ms Siglec F (PE), monoclonal	Thermo Fisher Scientific	Cat# 12-1702-80; clone 1RNM44N; Lot# 2252684; RRID: AB_2637129	(1:300)
Antibody	Armenian hamster anti-Ms FcεR1α (PE/Dazzle 594), monoclonal	BioLegend	Cat# 134331; clone MAR-1; Lot# B280348; RRID: AB_2687240	(1:300)
Antibody	Rat anti-Ms CD115 (PE-Cy7), monoclonal	BioLegend	Cat# 135523; clone AFS98; Lot# B268547; RRID: AB_2566459	(1:600)
Antibody	Rat anti-Ms F4/80 (BUV395), monoclonal	BD Biosciences	Cat# 565614; clone T45-2342; Lot# 1104580; RRID: AB_2739304	(1:150)
Antibody	Rat anti-Ms CD45 (APC-Cy7), monoclonal	BioLegend	Cat# 103115; clone 30-F11; Lot# NA; RRID: AB_312980	(1:150)
Antibody	Rat anti-Ms Ly-6C (PE-Cy7), monoclonal	BioLegend	Cat# 128017; clone HK1.4; Lot# B331355; RRID: AB_1732093	(1:600)
Antibody	Rat anti-Ms Ly-6G (Biotin), monoclonal	BioLegend	Cat# 127604; clone 1A8; Lot# B314606; RRID: AB_1186108	(1:600)
Antibody	Rabbit anti-*E. coli* ftsZ, polyclonal	Agrisera	Cat# AS10715; RRID: AB_10754647	(1:200)
Antibody	Rabbit anti-*E. coli* ompF, polyclonal	Biorbyt	Cat# orb308741; RRID: *NA*	(1:500)
Antibody	Goat anti-rabbit, polyclonal	LI-COR Biosciences	Cat# 925-68021; RRID: AB_2713919	(1:10,000)
Recombinant DNA reagent	pBAD28==pEMPTY (plasmid)	*Proietti et al., 2019*; *Santapaola et al., 2006*; *Scribano et al., 2014*	Ampicillin resistance	
Recombinant DNA reagent	pHND10==pAPY (plasmid)	*Proietti et al., 2019*; *Santapaola et al., 2006*; *Scribano et al., 2014*	Ampicillin resistance	
Sequence-based reagent	fD1	*Weisburg et al., 1991*	PCR primers	5'-AGA-GTT-TGA-TCC-TGG-CTC-AG-3'
Sequence-based reagent	fD2	*Weisburg et al., 1991*	PCR primers	5'-AGA-GTT-TGA-TCA-TGG-CTC-AG-3'
Sequence-based reagent	rP1	*Weisburg et al., 1991*	PCR primers	5'-ACG-GTT-ACC-TTG-TTA-CGA-CTT-3'
Commercial assay or kit	QIAquick Gel Extraction Kit	QIAGEN	Cat# 28706	
Commercial assay or kit	ATP Kit SL	BioThema	Cat# 144-041	
Commercial assay or kit	Cell Viability Kit with BD Liquid Counting Beads	BD Biosciences	Cat# 349480	
Commercial assay or kit	Microbial ATP Kit HS	BioThema	Cat# 266-112	
Commercial assay or kit	Intracellular ATP Kit HS	BioThema	Cat# 266-111	
Commercial assay or kit	ReliaPrep RNA Cell Miniprep System	Promega	Cat# Z6011	
Chemical compound, drug	Bacto Yeast Extract	Gibco	Cat# 212750	
Chemical compound, drug	Bacto Tryptone	Gibco	Cat# 211699	
Chemical compound, drug	Agar	Sigma-Aldrich	Cat# 05039-500G	

Appendix 1 Continued on next page

Appendix 1 Continued

Reagent type (species) or resource	Designation	Source or reference	Identifiers	Additional information
Chemical compound, drug	GoTaq G2 Green Master Mix	Promega	Cat# M782A	
Chemical compound, drug	Collagenase I (Col I)	Sigma-Aldrich	Cat# C0130-100MG	
Chemical compound, drug	Collagenase IV (Col IV)	Worthington	Cat# LS004189	
Chemical compound, drug	Collagenase D (Col D)	Roche	Cat# 11088858001	
Chemical compound, drug	DNAse I	Roche	Cat# 63792800	
Chemical compound, drug	Adenosine 5′-triphosphate disodium salt hydrate (ATP)	Sigma-Aldrich	Cat# 2383-1G	
Chemical compound, drug	Adenosine-5'-(γ-thio)-triphosphate, Tetralithium salt (ATPγs)	Jena Bioscience	Cat# NU-406-50	
Software, algorithm	GraphPad Prism v9.5.1	Prism GraphPad software	https://www.graphpad.com/	
Software, algorithm	FlowJo v10.8.1	FlowJo software	https://www.flowjo.com	
Software, algorithm	fastqc v0.11.9	*Babraham Bioinformatics, 2024*	http://www.bioinformatics.babraham.ac.uk/projects/fastqc/	
Software, algorithm	fastp v0.19.5	*Chen et al., 2018*	https://github.com/OpenGene/fastp RRID:SCR_016962	
Software, algorithm	STAR v2.7.10a_alpha_220818	*Dobin et al., 2013*	https://github.com/alexdobin/STAR RRID:SCR_004463	
Software, algorithm	subread v2.0.1	*Liao et al., 2014*	https://github.com/ShiLab-Bioinformatics/subread RRID:SCR_009803	
Software, algorithm	R v4.2.2	The R Project for Statistical Computing	https://cran.r-project.org	
Software, algorithm	RStudio v2022.07.2	RStudio Desktop	https://www.rstudio.com	
Software, algorithm	R package ggplot2 v3.4.3	*Wickham, 2016*	https://ggplot2.tidyverse.org	
Software, algorithm	R package readxl v1.4.3	*Wickham and Bryan, 2023a*	https://CRAN.R-project.org/package=readxl	
Software, algorithm	R package ggbreak v0.1.2	*Xu et al., 2021*	https://github.com/YuLab-SMU/ggbreak RRID:SCR_014601	
Software, algorithm	R package rstatix v0.7.2	*Kassambara, 2023*	https://CRAN.R-project.org/package=rstatix	
Software, algorithm	R package dplyr v1.0.10	*Wickham et al., 2023b*	https://CRAN.R-project.org/package=dplyr	
Software, algorithm	R package DESeq2 v1.38.3	*Love et al., 2014*	https://github.com/mikelove/DESeq2 RRID:SCR_015687	
Software, algorithm	R package ggrepel v0.9.3	*Slowikowski et al., 2023*	https://CRAN.R-project.org/package=ggrepel	
Software, algorithm	R package vegan v2.6–4	*Oksanen et al., 2022*	https://github.com/vegandevs/vegan RRID:SCR_011950	
Software, algorithm	R package pairwiseAdonis v0.4	*Arbizu, 2023*	https://github.com/pmartinezarbizu/pairwiseAdonis RRID:SCR_001905	

Appendix 1 Continued on next page

Appendix 1 Continued

Reagent type (species) or resource	Designation	Source or reference	Identifiers	Additional information
Software, algorithm	R package gprofiler2 v0.2.2	*Kolberg and Raudvere, 2023*	https://cran.r-project.org/web/packages/gprofiler2/index.html	
Software, algorithm	R package gplots v3.1.3	*Warnes et al., 2022*	https://CRAN.R-project.org/package=gplots	
Software, algorithm	R package viridis v0.6.3	*Ross et al., 2021*	https://sjmgarnier.github.io/viridis/ RRID:SCR_016696	
Other	Fixable Viability Dye eFluor506	Thermo Fisher Scientific	Cat# 65-0866-18	(1:600)
Other	Nalgene Rapid-Flow PES Filter Units	Thermo Scientific	Cat# 168-0045, 165-0045, 124-0045PK	
Other	Vybrant DiI Cell-Labeling Solution	Invitrogen	Cat# V22885	(1:100)
Other	DAPI	Sigma-Aldrich	Cat# D9542-5MG	(1:5000)
Other	Hoechst 33342	Thermo Fisher Scientific	Cat# H3570	(1:1000)
Other	LysoTracker	Invitrogen	Cat# L12492	(1:1000)